



Article

Integrating Climate Forecasts with the Soil and Water Assessment Tool (SWAT) for High-Resolution Hydrologic Simulations and Forecasts in the Southeastern U.S.

Vinit Sehgal ^{1,2} , Venkataramana Sridhar ^{1,*} , Luke Juran ³ and Jactone Arogo Ogejo ¹

¹ Department of Biological Systems Engineering, Virginia Polytechnic Institute and State University, Blacksburg, VA 24061, USA; vinit@vt.edu (V.S.); arogo@vt.edu (J.A.O.)

² Now at Water Management and Hydrological Science, Texas A&M University, College Station, TX 77840, USA

³ Department of Geography and the Virginia Water Resources Research Center, Virginia Polytechnic Institute and State University, Blacksburg, VA 24061, USA; ljuran@vt.edu

* Correspondence: vsri@vt.edu

Received: 25 July 2018; Accepted: 24 August 2018; Published: 29 August 2018



Abstract: This study provides high-resolution modeling of daily water budget components at Hydrologic Unit Code (HUC)-12 resolution for 50 watersheds of the South Atlantic Gulf (SAG) region in the southeastern U.S. (SEUS) by implementing the Soil and Water Assessment Tool (SWAT) model in the form of a near real-time, semi-automated framework. A near real-time hydrologic simulation framework is implemented with a lead time of nine months (March–December 2017) by integrating the calibrated SWAT model with National Centers for Environmental Prediction coupled forecast system model version 2 (CFSv2) weather data to forecast daily water balance components. The modeling exercise is conducted as a precursor for various future hydrologic studies (retrospective or forecasting) for the region by providing a calibrated hydrological dataset at high spatial (HUC-12) and temporal (1-day) resolution. The models are calibrated (January 2003–December 2010) and validated (January 2011–December 2013) for each watershed using the observed streamflow data from 50 United States Geological Survey (USGS) gauging stations. The water balance analysis for the region shows that the implemented models satisfactorily represent the hydrology of the region across different sub-regions (Appalachian highlands, plains, and coastal wetlands) and seasons. While CFSv2-driven SWAT models are able to provide reasonable performance in near real-time and can be used for decision making in the region, caution is advised for using model outputs as the streamflow forecasts display significant deviation from observed streamflow for all watersheds for lead times greater than a month.

Keywords: hydrologic modeling; soil moisture; SWAT; southeastern U.S.; CFSv2; HUC-12

1. Introduction

Global food security has come under severe threat, especially with the increasing human population and associated demand for freshwater resources and food production [1–3]. There are concerns over the increasing vulnerability of the southeastern U.S. (SEUS) to water-related conflicts due to continued growth in industrial, agricultural, metropolitan, and recreational water demand [4–6]. It is important to note that the SEUS is expected to have the largest absolute increase in population compared to any other region in the U.S. by 2030 [7,8]. Since water is a limited resource, it is likely that conflict for water sharing and use will become more commonplace and severe in the coming years.

Effective water resources planning has been very important for policymakers and engineers alike for this region, especially in the wake of several droughts in the region within a span of less than a decade. In the last fifteen years, the SEUS region has experienced an array of severe droughts, including severe and/or extreme drought conditions in early 2017 that impacted around half of the study region. These droughts have not only caused enormous strain on the agriculture and farms activities in the region but have also heightened instances of wildfires in the region, especially in the Appalachian region [9]. As the frequency of future hydrologic extremes is expected to increase, a reliable hydrologic forecast can be useful for the efficient planning of available water resources [10]. Previously, Lu et al. [11] developed an empirical model to estimate long-term annual actual evapotranspiration for forested watersheds in the SEUS. Limaye et al. [12] developed a macroscale hydrologic model for regional climate assessment studies in the SEUS. However, these studies do not address the watershed-scale variability in the region, which plays a crucial role in informed water resources management in the region.

Soil moisture and evapotranspiration (ET) are two important components of the hydrologic cycle and play an important role in the water, energy, and carbon cycle. ET plays an important role in linking the water, energy, and carbon cycles, and hence is crucial for the climate system and the hydrological cycle [13]. Accurate soil moisture and ET estimation is essential for delivering (or improving the quality of) reliable meteorological, hydrological, and environmental forecasts, such as precipitation [14], discharge estimates and prediction [15,16], identifying flash-flood prone areas and flood forecasting [17–19], the identification and characterization of droughts [20–22], and understanding soil–vegetation–atmosphere interactions [23,24] and boundary layer fluxes for improved water resource management [25,26]. However, both soil moisture and ET exhibit significant spatiotemporal variability across different scales owing to a range of processes, such as precipitation, and energy and water fluxes [27,28]. Factors including orography (on all scales), vegetation, and soil texture [29] also influence ET diurnally. There are no long-term observation data for soil moisture, unlike other hydrological variables, such as precipitation and streamflow, which are frequently recorded and reported. Additionally, large-scale remote sensing of ET using mechanistic or empirical models with the remotely sensed land surface and atmospheric properties [30–33] is popular; however, comparisons of the large number of remotely sensed ET datasets have indicated significant uncertainties associated with these products, with relative errors of 15–30% [33–35].

Currently, a combination of climate forecasts or reanalysis data with hydrological models is used to simulate the impacts of land use and climate change and other anthropogenic activities on the hydrological cycle [36,37]. These models provide a physical representation of the spatially variable hydrological processes [38] and key hydrological components such as ET and soil moisture. Previous studies have integrated hydrological models with a climate forecast dataset to forecast the state of hydrologic variables at seasonal/sub-seasonal time steps [39–42]. Utilizing information from seasonal climate forecasts and long-term climate predictions has proven to be of great interest to water planners and decision-makers to improve preparedness towards, and mitigation of, impacts due to climatic extremes [43,44]. Dynamical seasonal forecasting systems that are based on coupled atmosphere–ocean–land general circulation models (CGCMs) have been widely used for hydrologic forecasting in recent years [45,46]. Seasonal climate forecasts are useful in improving farmers' ability to mitigate adversities linked to climate extremes, particularly in rain-fed systems [41]. Farmers can use such forecasts to improve their crop diversification strategies and to decide which crops to plant [47,48]. Skillful prediction of the field-scale soil moisture is important to decide crop type, resource use, and crop insurance and contract renewals [44]. Application of the climate forecast system reforecast and reanalysis (CFSRR) products in hydrologic monitoring and prediction, seasonal soil moisture estimation, and understanding land-atmosphere interactions [49–54] has also been extensively explored. Very recently, Zhang et al. [55] integrated CFSv2 [56] with the Variable Infiltration Capacity (VIC) model and satellite data to predict drought in southwestern China and reported that CFSv2-coupled hydrological models only provide reliable soil moisture drought predictions for lead

times of 1 month. Recently, Kang and Sridhar [57] demonstrated the use of a CFSv2 weather forecast dataset in conjunction with VIC and SWAT models for improving drought prediction over the U.S.

However, most of these studies do not address the local landscape processes and biophysical heterogeneity to understand the watershed-scale hydrological responses to hydrological extremes, such as high/extreme precipitation or droughts, at local scales. Hydrological models implementable in a near real-time, semi-automated framework at the sub-watershed scale of 12-digit Hydrologic Unit Code (HUC-12) resolution are largely unavailable for the SAG region, despite growing water-related conflicts and growing demand for water for both agricultural and industrial applications. Recent studies by Kang and Sridhar [58] and Sehgal and Sridhar [59] highlight the importance of sub-watershed scale variability in hydrological processes and provide the impetus for high-resolution modeling with a focus on seasonal and sub-seasonal forecasting for the SAG region.

This study implements the SWAT model for 50 watersheds in the SEUS, calibrates and validates the models using the observed streamflow data, and provides retrospective hydrological simulations for the SAG region from 1982–2013 at a daily time step. Furthermore, the SWAT model is integrated with climate drivers from CFSv2 models to provide near real-time simulation and 9-month lead forecasts of hydrological variables from January 2014 to March 2017, and from April 2017 through to December 2017, respectively. The choice of SWAT model for simulating watershed hydrology is carried out by carefully evaluating the advantages of using semi-distributed hydrological models over lumped or fully distributed models, and the ease of implementation of the SWAT model compared to other similar, process-based models. While complete understanding of catchment hydrology may not be achievable using fully-distributed models, primarily due to the lack of quality dataset at a high spatial and temporal resolution, the lumped models are often criticized for not being capable of providing a reliable representation of the spatial variability in the land uses and hydrological processes [60]. Therefore, a semi-distributed model, such as SWAT, provides a tradeoff between fully-distributed and lumped models.

The objectives of this study are to provide high-resolution (HUC-12, daily), validated hydrological datasets for future application to the study region by implementing the following steps:

- (a) Develop the SWAT model to simulate various hydrologic variables at a daily time step for the South Atlantic-Gulf (SAG) region of the southeastern U.S. (SEUS) at HUC-12 (12-digit Hydrologic Unit Code) resolution.
- (b) Two-fold validation of the dataset using observed streamflow and in-situ soil moisture dataset.
- (c) Develop a near real-time forecasting framework with a forecast window of 9 months to forecast the water balance components at the sub-watershed scale using the calibrated SWAT model initialized with climate drivers from CFSv2 at a daily time step.

The purpose of this study is to develop models to represent the sub-watershed scale processes at a high resolution (HUC-12), which can be used under a dynamic setting to develop water resources scenarios for the routine assessment of water availability with relative ease over sub-continental scales.

2. SWAT Model

Model Background

The Soil and Water Assessment Tool (SWAT) is used in this study to simulate the hydrologic cycle at a sub-watershed scale. SWAT operates in a continuous-time mode, and is a process-based, semi-distributed, comprehensive water balance model [61–63]. Simulations from the SWAT model incorporate weather, hydrology, sedimentation, soil temperature, plant growth, nutrients, pesticides, and land management [64]. The model uses precipitation, radiation, and temperature, along with elevation, soil, and land cover/land use data as inputs for simulating surface and sub-surface hydrological processes. The unique combinations of soil type and land use (and slope if desired) are lumped as a hydrologic response unit (HRU) that dictates the physical response of the watershed to

climate drivers. Thus, each sub-watershed is divided into several HRUs and the land component of the hydrologic cycle is modeled for each HRU. Surface runoff is estimated in the model using the Soil Conservation Service Curve Number (SCS-CN) method [65].

A two-layer structure represents the aquifer system in SWAT, where the first layer represents the shallow aquifer and can interact with the surface water or add to the groundwater flow, whereas the water in the deeper layer is considered to be out of the system. These fluxes are calculated as a lumped average value for the entire HRU. The surface runoff is routed to the outlet to the watershed as streamflow. SWAT uses a temperature dependent equation like the Penman-Monteith equation for estimating the potential evapotranspiration, while plant growth is modeled using a modified Environmental Policy Integrated Climate (EPIC) model to estimate actual plant transpiration [66]. For more details on the SWAT model, readers are further referred to the SWAT literature database for literature on SWAT for various hydrological modeling applications [67].

3. Study Area and Model Dataset

3.1. Study Area

This study evaluates the hydrology of the South Atlantic-Gulf (SAG) region in the southeastern U.S., as shown in Figure 1. The geographic area of the SAG region spans an area of 724,326 square kilometers and encompasses Florida (FL) and South Carolina (SC), and parts of Georgia (GA), Alabama (AL), Louisiana (LA), Mississippi (MI), North Carolina (NC), Tennessee (TN), and Virginia (VA) [68]. The western part of the SAG region is bounded by Appalachia and is predominantly forested with low development and urbanization, high elevation, and silty soil. The central and southern parts of the SEUS are dominated by woody wetlands, open spaces, and cultivated crops. The southern tip of Florida is dotted with water bodies and wetlands, with some areas of cultivated crops and developed spaces. The soil in the coastal plains has a high percentage of sand and low percentages of clay and silt (Figure 2).

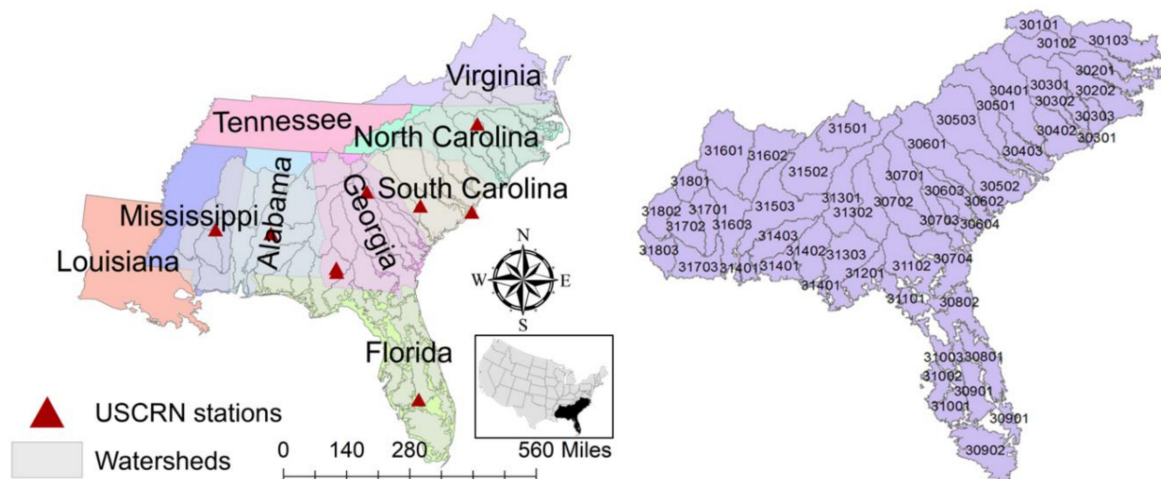


Figure 1. (Left) Map showing the location of the study area. Watersheds in the South Atlantic-Gulf (SAG) region are highlighted in grey shade. The soil moisture measurement stations from the U.S. Climate Reference Network (USCRN) are shown with red triangles. The inset shows the location of the entire study region over the map of the contiguous U.S. (Right) Map showing the modeled watersheds with their respective numbers.

The SAG region is identified using a two-digit number “03” in the HUC system. This region is divided into 18 basins, each distinguished using a four-digit HUC identifier ranging from 0301–0318. These HUC-4 basins are further divided into 50 watersheds, and the SWAT model is used to model

the hydrology for each watershed at a HUC-12 resolution. HUC-12 is the 12-digit identifier for the sub-watersheds. Out of a total of 7453 HUC-12 sub-watersheds provided by the National Hydrography Database plus (NHD+) in the study area, the SWAT model delineated 7391 sub-watersheds for the entire SAG region, thus ensuring high spatial resolution of the simulations. Table 1 provides the list of 18 basins in the SAG region; each is referred to by its HUC-4 identifier and the name of the sub-watersheds with the outlet matching with the U.S. Geological Survey (USGS) streamflow-gauging stations. Note that the authors provide the watershed numbers only for ease of reference and the identification of these watersheds in the study, and they are not to be confused with the watersheds at HUC-6, which are larger than these watersheds in most cases.

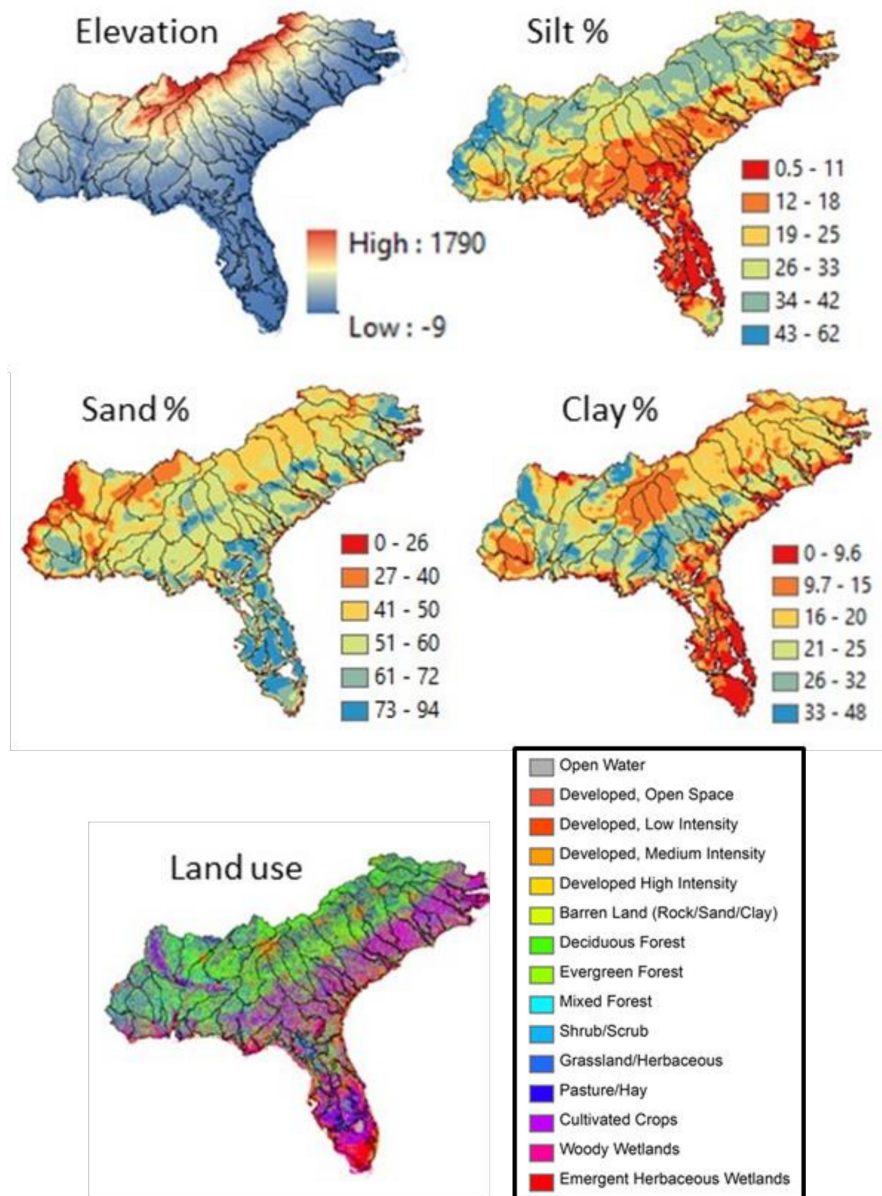


Figure 2. Elevation, percentage of silt, sand and clay, and land use (NLCD 2001) in the study area.

Table 1. CFSv2 monthly ensembles with respective initial day of the month for four members initialized at 00Z, 06Z, 12Z, and 18Z [69].

| Initialization Month | Total Members | Initialization Days |
|----------------------|---------------|--------------------------|
| January | 28 | 1, 6, 11, 16, 21, 26, 31 |
| February | 20 | 5, 10, 15, 20, 25 |
| March | 24 | 2, 7, 12, 17, 22, 27 |
| April | 24 | 1, 6, 11, 16, 21, 26 |
| May | 28 | 1, 6, 11, 16, 21, 26, 31 |
| June | 24 | 5, 10, 15, 20, 25, 30 |
| July | 24 | 5, 10, 15, 20, 25, 30 |
| August | 24 | 4, 9, 14, 19, 24, 29 |
| September | 24 | 3, 8, 13, 18, 23, 28 |
| October | 24 | 3, 8, 13, 18, 23, 28 |
| November | 24 | 2, 7, 12, 17, 22, 27 |
| December | 24 | 2, 7, 12, 17, 22, 27 |

3.2. Model Dataset

The basic drivers for the SWAT model were the U.S. Geological Survey (USGS)-derived Digital Elevation Model (DEM), State Soil Geographic (STATSGO) soil data, and land use/land cover data from the National Land Cover Data (NLCD) 2011 [70]. Weather data (precipitation and temperature) is obtained from the National Centers for Environmental Prediction (NCEP) Climate Forecast System Reanalysis (CFSR) data [56,71,72]. The reanalysis data is available for a period of 36 years from 1979 to 2013 and can be accessed through the global weather database for SWAT (URL: <https://globalweather.tamu.edu>). Studies have previously evaluated the performance of the reanalysis product and have reported satisfactory performance in watershed-scale modeling using the dataset [72–75]. One USGS station for each watershed was chosen for calibrating and validating the streamflow generated using the SWAT model (listed in Table 1). The land use, soil, and elevation data used in the models are shown in Figure 2.

The CFSR is extended as an operational, real-time product that forecasts the atmospheric variables with a lead time of nine months and was initialized multiple times a day, and on different days of the month (Table 2). Precipitation and temperature time series were obtained from CFSv2 data from 1 April 2011, through to 19 December 2017 by using the first instance of the CFSv2 model dataset from 1 April 2011, through to 12 March 2017, and a 9-month forecast data was then obtained from the most recent initialization (12 March 2017 in this study). Figure 3 provides a schematic of data assimilation for the study. The red ellipse highlights the model run for each initialization, which was used for SWAT model implementation, with a total number of K initializations from 1 April through to 12 March 2017.

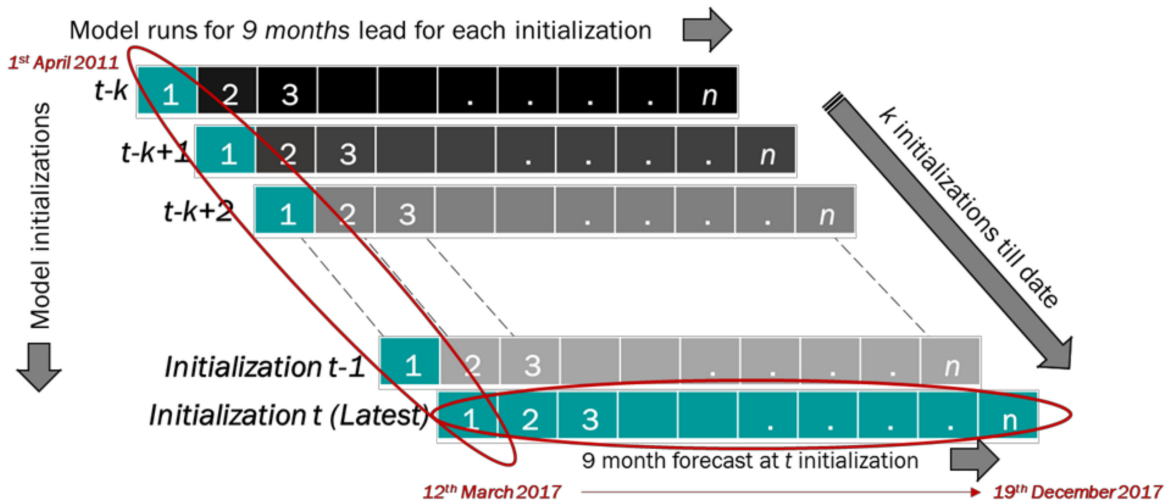


Figure 3. Data assimilation scheme for precipitation and temperature from the CFSv2 dataset. Precipitation and temperature time series were obtained from 1 April 2011, through to 12 March 2017, for the first instance of the CFSv2 model runs. Then, 9-month forecast data were obtained from the most recent initialization.

Table 2. List of the 18 basins in the South Atlantic-Gulf region identified with a four-digit Hydrologic Unit Code and a six-digit identification number (not to be confused with HUC-6) for the constituent watersheds along with their respective outlet USGS stations (reproduced with permission from Sehgal and Sridhar [59]).

| Basin | USGS Station | Watershed | River/Basin | Basin | USGS Station | Watershed | River/Basin | |
|----------|--------------|-----------|---------------------------|--------------------|--------------|-----------|------------------|----------------------|
| 0301 | 02066000 | 030101 | Roanoke | 0309 | 02292900 | 030902 | Caloosahatchee | |
| | 02075500 | 030102 | Dan | 0310 | 02296750 | 031001 | Peace | |
| | 02047000 | 030103 | Nottoway | | 02301500 | 031002 | Alafia | |
| 0302 | 02084000 | 030201 | Tar | | 02313000 | 031003 | Withlacoochee | |
| | 02091814 | 030202 | Neuse | 0311 | 02323500 | 031101 | Suwannee | |
| 0303 | 02134500 | 030301 | Lumber | | | 02317500 | 031102 | Alapaha |
| | 02106500 | 030302 | Black | 0312 | 02330150 | 031201 | Ochlockonee | |
| | 02108000 | 030303 | NE Cape fear | | | 02338000 | 031301 | Chattahoochee |
| 0304 | 02129000 | 030401 | Pee Dee | 0313 | 02350512 | 031302 | Flint | |
| | 02134500 | 030402 | Lumber | | | 02358700 | 031303 | Apalachicola |
| | 02132000 | 030403 | Lynches | 0314 | 02369600 | 031401 | Yellow | |
| 0305 | 02147020 | 030501 | Catawba | | | 02366500 | 031402 | Choctawhatchee |
| | 02169500 | 030502 | Congaree | | | 02374250 | 031403 | Conecuh |
| | 02175000 | 030503 | Edisto | 0315 | 02397000 | 031501 | Coosa (Rome) | |
| 0306 | 02197000 | 030601 | Savannah | | | 02407000 | 031502 | Coosa (Childersburg) |
| | 02198000 | 030602 | Barrier Creek | | | 02428400 | 031503 | Alabama |
| | 02202500 | 030603 | Ogeechee | 0316 | 02448500 | 031601 | Noxubee | |
| | 02203000 | 030604 | Canoochee | | | 02466030 | 031602 | Black warrior |
| 0307 | 02223500 | 030701 | Oconee | | 02469761 | 031603 | Tombigbee | |
| | 02215000 | 030702 | Ocmulgee | 0317 | 02478500 | 031701 | Chickasawhay | |
| | 02225500 | 030703 | Ohoopee | | | 02474500 | 031702 | Tallahala |
| | 02228000 | 030704 | Satilla | | | 02479300 | 031703 | Red Cr. |
| | 0308 | 02234000 | 030801 | St. Johns (Geneva) | 0318 | 02482550 | 031801 | Pearl (Carthage) |
| 02244040 | | 030802 | St. Johns (Buffalo bluff) | | | 02488500 | 031802 | Pearl (Monticello) |
| 0309 | 02270500 | 030901 | Arbuckle Cr. | | 02489500 | 031803 | Pearl (Bogalusa) | |

4. Methods

4.1. Modeling Framework

The SWAT model was calibrated from 2003 through to 2010 with a three-year warm-up period (2000 through to 2002) and was validated from 2011 through to 2013. The parameterization of the models was carried out in ArcSWAT 2010 (<https://swat.tamu.edu/software/arcswat/>). The sequential uncertainty fitting-2 (SUFI-2) algorithm [76–78] was employed to calibrate the model parameters using the SWAT-CUP (calibration/uncertainty or sensitivity program) interface. The SUFI-2 algorithm was used based on its ability to provide the best fitness while accounting for the high degree of uncertainty between the simulated and observed dataset [79]. The parallel processing routine [80] available with SUFI-2 was used while simulating 1000 iterations for each watershed. Once the calibrated parameters were obtained from SWAT-CUP, a MATLAB-based script was written to update SWAT input-output files and run the SWAT model with calibrated parameters for the validation period and re-run the SWAT model for the period of January 1982 through to December 2013 with a three-year warm-up period (1979 through to 1981) to obtain the long-term hydrologic variables for this study.

4.2. Calibration of SWAT Model Using the Sequential Uncertainty Fitting (SUFI)-2 Algorithm

A set of 24 parameters were chosen for calibration to address various hydrologic components of the watershed, such as surface runoff (curve number, soil and plant evaporation, surface runoff and Manning's coefficient, and available soil water capacity, etc.), baseflow (groundwater "revap", aquifer–soil interaction, depth of water in the shallow aquifer, time for water leaving the root zone to reach the shallow aquifer, and deep aquifer percolation), storm water (channel hydraulic conductivity, stormflow lag time, etc.), snow (snowmelt rate, snow temperature, etc.), etc. Nash Sutcliffe Efficiency (NSE) [81] was chosen as the performance criteria for the models. The choice and effect of these parameters are very well documented in the SWAT literature [62–87], and the selected parameters are consistent with the aforementioned studies. The same set of selected 24 parameters were calibrated for each watershed as a measure to achieve reasonable performance for watershed-scale streamflow simulation and a broad representation of the geographical and hydrological variability of the region. These parameters were carefully selected to address both wetland/riparian watershed hydrology [65–89] and inland basin characteristics, with special regard to the heterogeneity in elevation, vegetation, and soils of the study region.

A list and a brief description of the 24 parameters selected for this study is provided in Table 3. In order to provide realistic estimates of the parameter space for each watershed, the initial parameters were fine-tuned before implementing calibration in the interest of computational ease and time. The minimum and maximum values provided in Table 3 provided the parameter range used for the search of the optimum value of the respective parameter in calibration. Since the total number of watersheds used in this study made it difficult to provide the calibrated values in the form of a table, Figure 4 provides the spatial map of the calibrated values of the parameters used in this study.

Table 3. Selected parameters for calibrating the SWAT Model using Sequential Uncertainty Fitting 2 (SUFI-2) algorithm for the daily discharge dataset from 1 January 2003 to 31 December 2010. The minimum and maximum parameter range for the SUFI-2 optimization is provided in the table. The calibrated values are shown in Figure 4.

| Class | Name | Description | Method Used | Min. | Max. |
|-------|-----------|---|--------------|-------|------|
| HRU | ESCO | Soil evaporation compensation factor (unitless) | Replace (v) | 0 | 1 |
| | EPCO | Plant evaporation compensation factor (unitless) | Relative (r) | −0.2 | 0.2 |
| | HRU_SLP | Average slope steepness (mm/mm) | Relative (r) | −0.2 | 0.2 |
| | OV_N | Manning's "n" value for overland flow | Replace (v) | 0.01 | 30 |
| | SLSUBBSN | Average slope length (m) | Relative (r) | −0.2 | 0.2 |
| MGT | CN2 | Initial SCS curve number for moisture condition II (unitless) | Relative (r) | −0.2 | 0.2 |
| | BIOMIX | Biological mixing efficiency (unitless) | Relative (r) | −0.2 | 0.2 |
| SOL | SOL_AWC | Available water capacity of the soil layer (mm/mm) | Relative (r) | −0.2 | 0.2 |
| | SOL_BD | Moist bulk density (mg/m ³ or g/cm ³) | Replace (v) | 0.9 | 2.5 |
| BSN | SMTMP | Snowmelt base temperature (°C) | Relative (r) | −0.2 | 0.2 |
| | SMFMN | Melt factor for snow on Dec 21 (mm H ₂ O/°C·day) | Relative (r) | −0.2 | 0.2 |
| | SMFMX | Melt factor for snow on June 21 (mm H ₂ O/°C·day) | Relative (r) | −0.2 | 0.2 |
| | MSK_CO1 | Calibration coefficient used to control the impact of storage time constant (K _m) for normal flow when K _m is calculated for the reach | Relative (r) | −0.2 | 0.2 |
| | MSK_CO2 | Same as above, but for low flows | Relative (r) | −0.2 | 0.2 |
| | SURLAG | Surface runoff lag coefficient | Replace (v) | 0.05 | 24 |
| GW | GWQMN | Threshold depth of water in the shallow aquifer required for return flow to occur (mm) | Replace (v) | 0 | 5000 |
| | GW_REVAP | Groundwater reevaporation coefficient (unitless) | Replace (v) | 0.02 | 0.2 |
| | GW_DELAY | Groundwater delay (days) | Replace (v) | 0 | 500 |
| | ALPHA_BF | Base flow alpha factor (days) | Replace (v) | 0 | 1 |
| | RCHRG_DP | Groundwater recharge to deep aquifer (fraction) | Relative (r) | −0.2 | 0.2 |
| | REVAPMN | Threshold depth of water in the shallow aquifer for reevaporation to occur (mm) | Relative (r) | −0.2 | 0.2 |
| RTE | CH_N2 | Manning coefficient for channel (unitless) | Replace (v) | −0.01 | 0.3 |
| | CH_K2 | Effective channel hydraulic conductivity (mm/h) | Replace (v) | −0.01 | 500 |
| | ALPHA_BNK | Baseflow alpha factor for storage (days) | Replace (v) | 0 | 1 |

To highlight the influence of the land use characteristics on the estimation of the model parameters, a comparison is made between some of the selected model parameters, namely CN2, BIOMIX, HRU_SLP, and ESCO (for brevity), with the percentage of land use under five classes, namely developed land, forest, cultivated, grass/shrub/hay, and wetlands, at a watershed scale in Figure 5. It can be observed that there was a strong influence of land use characteristics on the model parameters. A higher HRU_SLP corresponded to the higher percentage of forest areas, as much of the Appalachian mountain region is heavily forested. A higher value of BIOMIX corresponded to the higher percentage of forest or grasslands and a low amount of development in watersheds. High ESCO values corresponded to forested watersheds and a higher percentage of wetland areas, especially in the coastal watersheds. CN2 was impacted by a combination of factors, including a higher percentage of developed or cultivated areas or a higher percentage of wetlands. In some cases, CN2 also corresponded to a high forest cover percentage. However, this can be explained by the mountainous topography of these watersheds. It was observed that while the values of these parameters varied for each watershed (Figure 4), the overall performance of the models for streamflow simulation during calibration and validation periods at all 50 outlets was satisfactory with the given set of model parameters. The strong influence of land use, topography, soil type, and other watershed scale characteristics could be seen on the spatial variability of these parameters. For instance, predominantly forested areas showed higher values for BIOMIX due to the higher redistribution of soil constituents from biota (for example earthworms, etc.) compared to wetlands or developed watersheds; HRU_SLP values were higher for mountainous regions compared to plains and coastal areas; SLSUBBSN was found to be higher for coastal watersheds due to the low gradient. OV_N showed variability based on the surface characteristics of the overland flow and varied from basin to basin. Other important parameters, such as CN2, SOL_AWC, ALPHA_BF, and EPCO, show significant spatial variability. A combination of these factors determined the response of a watershed to precipitation and the resultant discharge and storage. For example, low ALPHA_BF numbers signified a slow response to changing moisture conditions in the baseflow under no recharge to the watershed, whereas higher CN2 numbers signified higher runoff for a given precipitation amount. Interaction with groundwater (GW_DELAY, GW_QMN, and GW_REVAP) and runoff play a major role in the partitioning of precipitation in the watershed into runoff, soil, and groundwater storage. A slow surface-aquifer interaction, coupled with a high curve number, led to high values of discharge.

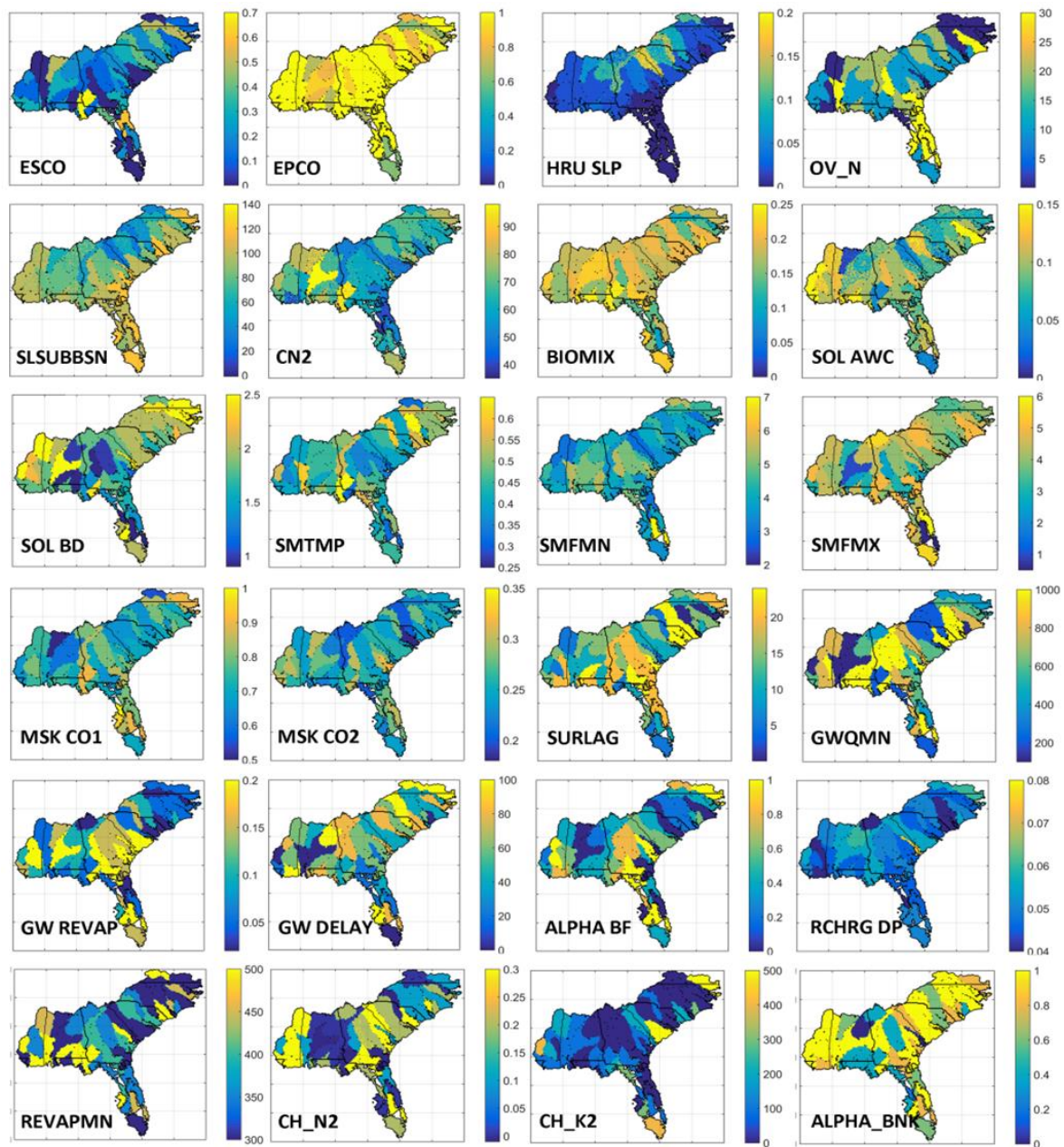


Figure 4. Maps of SWAT parameters calibrated using the SUFI-2 algorithm.

4.3. Performance Evaluation of the SWAT Model

The SWAT-simulated streamflow is compared with the observed discharge data from the selected USGS gauging stations for the purpose of performance assessment. Three statistical performance indices, namely the coefficient of determination (R^2), the normalized root mean square error (NRMSE), and Willmott's Index (WI) [90,91], were used for quantitative assessment of the results. The NRMSE were normalized values of the RMSE to a range of [0, 1] to facilitate comparison of the model performance with other watersheds. For all selected indices, values closer to 1 indicate better performance. Latest studies have proposed spatial-pattern-oriented model calibration and performance indices (based on simulating the spatiotemporal variability of the dataset) [92,93] based on satellite observations and/or advanced measurement and monitoring capabilities in the study region [94]. However, a lack of such a dataset at the spatial and temporal resolution of this study restricted the validation of the dataset to sub-watershed scale validation of observed streamflow from USGS,

and validation of the seasonal and sub-seasonal variability of the simulated soil moisture using in-situ stations.

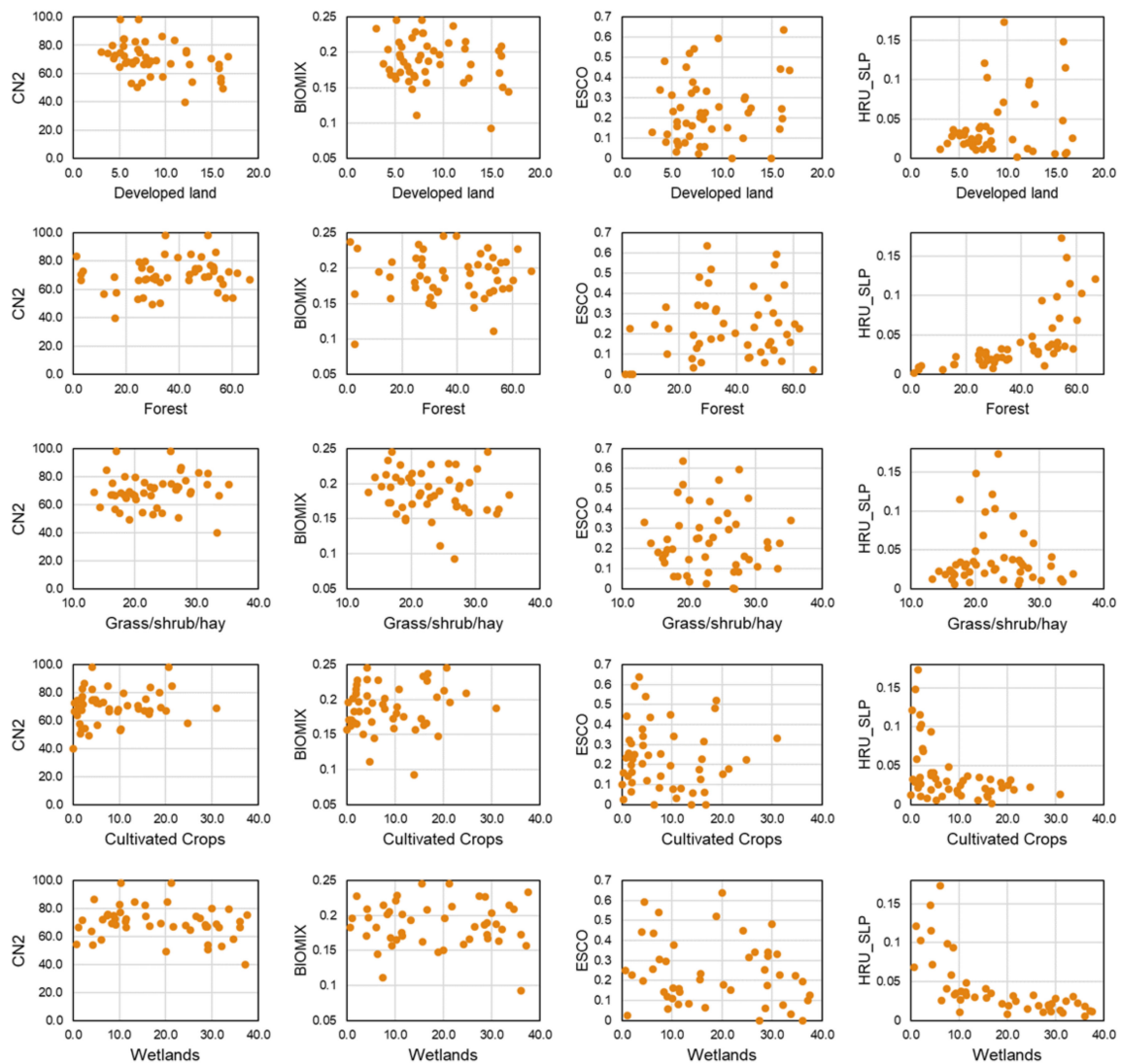


Figure 5. Scatter plot of CN2, BIOMIX, HRU SLP, and ESCO with the percentage of dominant land-use types for the 50 watersheds in the study region.

4.4. Hydrologic Simulations Using the CFSv2-Integrated Calibrated SWAT Model

The calibrated SWAT model was integrated with CFSv2-derived variables from April 2011 through to December 2017 with a warm-up period of 3 years, thus providing simulation outputs from January 2014 through to December 2017. Seamless daily simulation outputs were obtained from January 1982 through to December 2017 by combining the retrospective model simulations from the CFSR-integrated SWAT model and the CFSv2-integrated SWAT model. SWAT-CFSv2 model outputs (soil water, evapotranspiration, potential evapotranspiration, surface runoff, watershed precipitation, etc.) for the period of April 2011 through to March 2017 were obtained in near real-time mode since the input meteorological data was taken from the first CFSv2 model runs, whereas SWAT-CFSv2 output data from March through to December 2017 were the forecasted model outputs.

4.5. Water Balance Analysis

This study follows Sridhar and Hubbard [95] and Singh et al. [96] in studying the water balance of the study region. The fundamental water balance equation can be expressed as:

$$\frac{\partial S}{\partial t} = PREC + I - ET - R - D \quad (1)$$

where S is the soil water in the root zone (mm); t is the time (day); $PREC$ is precipitation (mm/day); I is the irrigation (mm/day); ET is the actual evapotranspiration (mm/day); R is runoff (mm/day); and D is the drainage below the root zone (mm/day).

The daily estimates of water balance components for each watershed were added to the monthly totals and subsequently used to estimate the monthly water balance components for each watershed. The change in soil water storage ΔSW was calculated by subtracting the storage of the previous month from the current month's (t) storage.

$$\Delta SW = SW_t - SW_{t-1} \quad (2)$$

The actual ET was computed for each month using the change in precipitation and soil water storage

$$\begin{aligned} ET &= PREC - \Delta SW, \text{ if } \Delta SW \leq 0 \\ ET &= PREC + \Delta SW, \text{ if } \Delta SW > 0 \\ ET &= PET, \text{ if } \Delta SW > 0 \end{aligned} \quad (3)$$

The difference between potential ET (PET) and actual ET , was used to calculate the water deficit. Surplus water was estimated by subtracting ET from the sum of the soil storage and precipitation.

$$\text{Deficit} = PET - ET \text{ Surplus} = PREC - (ET - \Delta SW) \quad (4)$$

5. Results and Discussion

5.1. Streamflow Validation

A spatial representation of the SWAT models in simulating stream discharge is provided in Figure 6. It can be seen that while the performance of the SWAT models can be deemed satisfactory for most inland gauging stations, the performance of the models was weak in the coastal marshlands, especially in Florida. It is to be noted that at these gauging locations, the observed streamflow discharge was heavily influenced by tides. These tidal activities added a secondary oscillatory component in the streamflow records. These tidal cycles corresponded to a period of 24.84 h and successive averaging in daily computations of the recorded data by USGS led to a secondary oscillatory component in the data with a time period of about two weeks. These oscillations, which were unrelated to the watershed hydrology, were often missed by the SWAT models, leading to a high degree of discrepancy between the observed and the simulated streamflow. Furthermore, extensive basin management and regulation practices could also lead to poor simulations by the SWAT models as water management practices were not explicitly included in the SWAT model setup in this study. Additionally, it was observed that the performance of the SWAT model was better for larger, downstream watersheds due to reduced intermittency and sustained flow regimes. A combination of these factors caused the deviation of SWAT-simulated values from the observed dataset. For a vast majority of watersheds (approximately 30 inland watersheds), the models showed $R^2 = [0.45, 0.68]$, $NRMSE = [0.07, 0.1]$, and $WI = [0.45, 0.68]$ for the calibration and validation datasets at daily time step, respectively. The performance of the models for the rest of the SAG region was assessed to be satisfactory based on the findings of several other studies conducted in various parts of the SEUS, such as Virginia [58], the coastal plain of southwestern Georgia [97], low-gradient watersheds in South Carolina [98], etc.

5.2. Validation of Soil Moisture Data

Given the importance of long-term high-resolution soil moisture (SM) simulations for the study region, a comparison was made between the SWAT simulated SM with nine in-situ stations located within the study area. These soil moisture stations belong to the U.S. Climate Reference network (USCRN), which provide observations for five standard depths, i.e., 5 cm, 10 cm, 20 cm, 50 cm, and 100 cm. Weekly averaged values of the observed SM from USCRN stations were compared with the corresponding values of the area averaged, sub-watershed scale SM from the total rooting depth of the SWAT models after suitable conversion to volumetric units. Figure 1 provides the geographic locations of the USCRN stations selected for this study. The SM time series for five soil sensor depths for one of the USCRN stations used in the study area are provided in the supplementary material. In order to capture the general dynamics of the SM across the total rooting depth, this study used in-situ soil moisture data from three sensor depths, i.e., 10 cm, 20 cm, and 50 cm, for simultaneous comparison with area-averaged total rooting depth soil moisture simulations from the SWAT models for the respective sub-watershed. For ease of comparison, a suitable conversion was applied to the SWAT simulated soil moisture to obtain the volumetric SM content using the total rooting depth of the respective sub-watershed.

Figure 7 provides a comparison of the in-situ and simulated SM values for three sensor depths. The days with the missing in-situ data were ignored in the analysis. Strong seasonality was evident from the plots, where SM values could be observed to decline in the summer months and recovered in the winter months. Table 4 provides the comparison between the SWAT simulated SM with the in-situ measurements using correlation and RMSE as performance indices. It can be observed that the performance of the SM simulation was satisfactorily high except for the coastal watersheds (in Florida and another in South Carolina) for reasons highlighted in Section 5.1. While for most locations, the general inter-seasonal dynamics was captured by the SWAT simulated SM, there could be a systematic bias in the simulations or errors in capturing the extreme high and low values. Despite relatively high values of RMSE in some stations due to systematic bias in the simulations, high values of correlation between the in-situ and simulated SM provided the opportunity to use the simulated SM in applications where the general trend of the dataset and deviation from the retrospective values were of importance. This made SM simulations from SWAT useful for retrospective drought analysis and/or real-time monitoring, as used by Sehgal and Sridhar [59].

However, there were two important considerations in interpreting the comparison of model and in-situ SM data: (i) difference in the scale of the SWAT simulations and in-situ observations, and (ii) difficulty in determination of the representative sensor depth for capturing the rooting depth soil moisture dynamics. While point-scale measurements typically have a support scale of a few centimeters, the SWAT models provided a lumped estimate of SM simulations at the HRU scale. This difference in scale between the in-situ and SWAT simulated SM may have added systematic bias in the two datasets. Furthermore, moisture distribution within a soil profile is a non-linear and complex process with a strong influence of a combination of factors like local topography, vegetation, soil composition, soil hydraulic properties, etc. This makes it difficult to assign a representative soil depth to capture the root-zone soil moisture dynamics using the in-situ measurements.

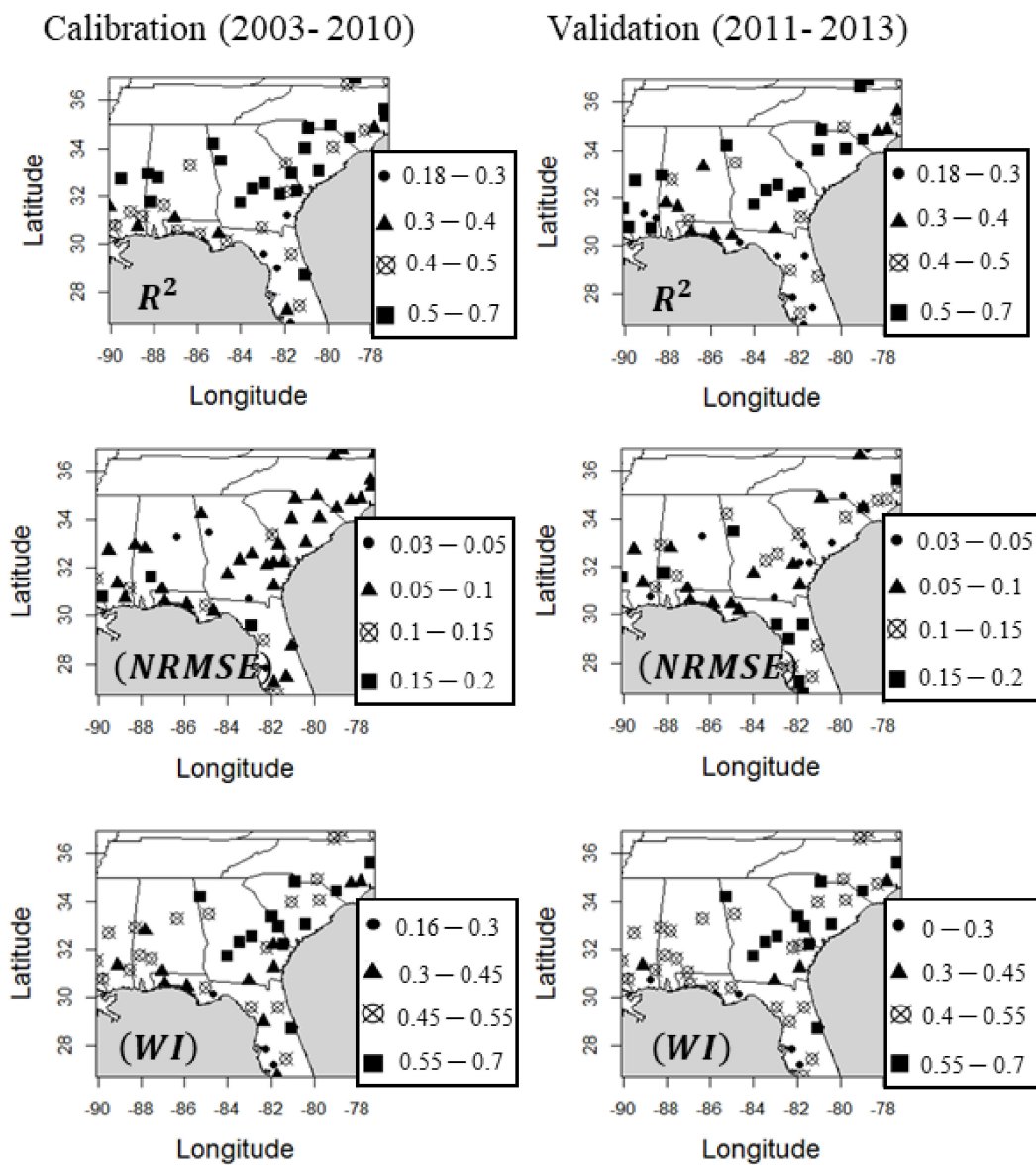


Figure 6. Values of the statistical performance indices for the 50 USGS streamflow gauging stations selected for this study for the calibration (2003–2010) and validation (2011–2013) periods. (Statistical indices are defined as: $R^2 = \frac{\sum_{i=1}^n (O_i - \bar{O})(P_i - \bar{P})}{\sqrt{\sum_{i=1}^n (O_i - \bar{O})^2} \sqrt{\sum_{i=1}^n (P_i - \bar{P})^2}}$, $NRMSE = \frac{\sqrt{\frac{1}{n} \sum_{i=1}^n (O_i - P_i)^2}}{(Max(O) - Min(O))}$, $WI = 1 - \frac{\sum_{i=1}^n |(P_i - \bar{O}) - (O_i - \bar{O})|}{\sum_{i=1}^n (|(P_i - \bar{O})| + |(O_i - \bar{O})|)}$ [90], where O_i and P_i are the observed and estimated discharge time series and n is the number of data points).

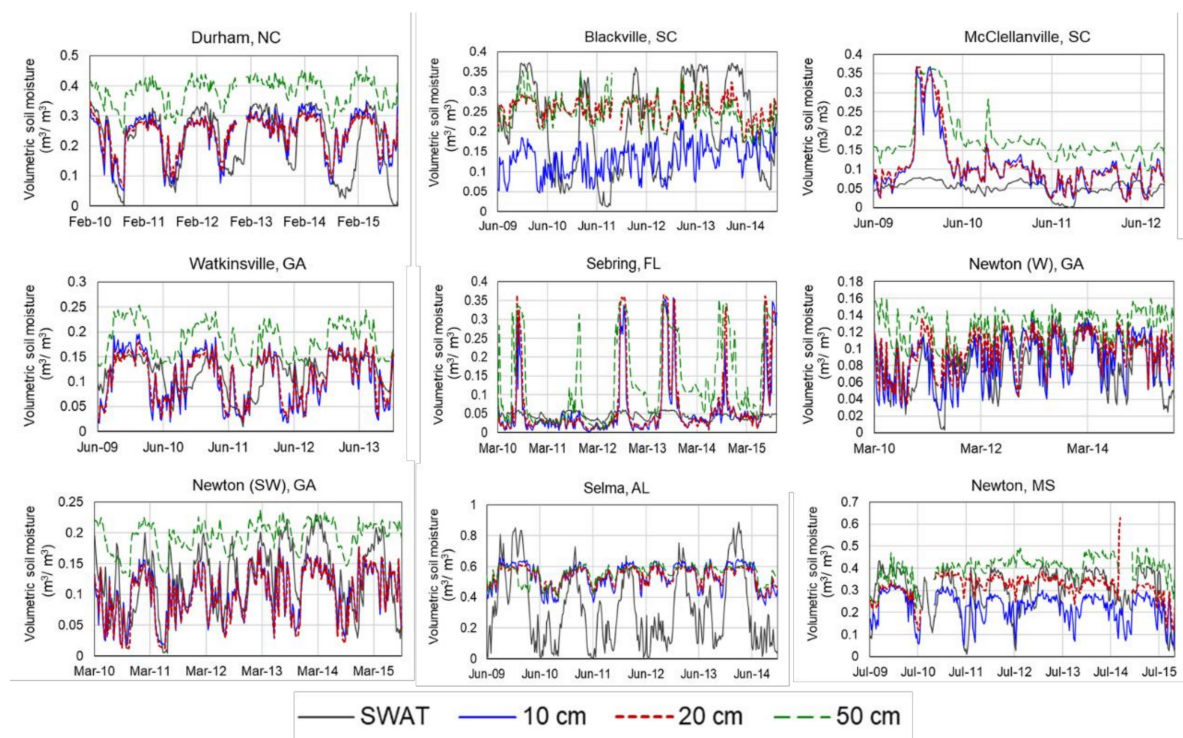


Figure 7. Comparison of weekly in-situ soil moisture and the SWAT simulated soil moisture (in volumetric units) from the corresponding HUC-12 resolution sub-watershed for three sensor depths (10 cm, 20 cm, and 50 cm) at nine locations.

Table 4. Performance evaluation of the sub-watershed (HUC-12) scale SWAT-simulated soil moisture (in volumetric units) using in-situ soil moisture observations for three sensor depths (10 cm, 20 cm, and 50 cm) at nine locations.

| Station location (Lat, Lon) | Correlation | | | RMSE (m^3/m^3) | | |
|------------------------------------|-------------|-------|-------|----------------------------------|-------|-------|
| | 10 cm | 20 cm | 50 cm | 10 cm | 20 cm | 50 cm |
| Durham, NC (35.97, -79.09) | 0.658 | 0.681 | 0.749 | 0.227 | 0.224 | 0.372 |
| Blackville, SC (33.36, -81.33) | 0.324 | 0.345 | 0.279 | 0.131 | 0.125 | 0.020 |
| McClellanville, SC (33.15, -79.36) | 0.550 | 0.543 | 0.502 | 0.080 | 0.017 | 0.076 |
| Watkinsville, GA (33.78, -83.39) | 0.581 | 0.602 | 0.643 | 0.043 | 0.012 | 0.078 |
| Sebring, FL (27.15, -81.37) | 0.424 | 0.436 | 0.533 | 0.081 | 0.029 | 0.100 |
| Newton (W), GA (31.31, -84.47) | 0.552 | 0.564 | 0.481 | 0.029 | 0.017 | 0.033 |
| Newton (SW), GA (31.19, -84.45) | 0.579 | 0.594 | 0.628 | 0.051 | 0.007 | 0.098 |
| Selma, AL (32.33, -86.98) | 0.726 | 0.673 | 0.339 | 0.290 | 0.029 | 0.045 |
| Newton, MS (32.34, -89.07) | 0.582 | 0.348 | 0.265 | 0.107 | 0.099 | 0.095 |

5.3. Near Real-Time Daily Simulations Using the CFSv2-Integrated SWAT Model

To evaluate the performance of the CFSv2-integrated SWAT model using near real-time meteorological data from CFSv2 model outputs, the time series plots of the observed and simulated discharges for the Roanoke, Pearl, Satilla, and Coosa Rivers are shown in Figure 8. The R^2 values of the simulation are provided in the figure. It can be seen that the performance of the models for these watersheds was similar to the calibration and validation results, as discussed in the previous sections. The 9-month forecasts of simulated discharge were compared with the observed discharge values for the four watersheds, which are provided in Figure 9. It can be observed from Figure 9 that while the near real-time simulation using SWAT-CFSv2 models provided a realistic estimate of the discharge, the simulations using the forecasted meteorological dataset may not be considered

to be reliable. The observed and forecasted river discharge values could be observed to be within a close range only up to a lead of approximately 1 month, beyond which the simulated and observed discharge show a high degree of disagreement. This issue could be countered by updating the SWAT model with every new initialization of CFSv2 (or a few times each month) in order to update the model state with the latest forcing dataset for reliable forecasts of hydrological variables.

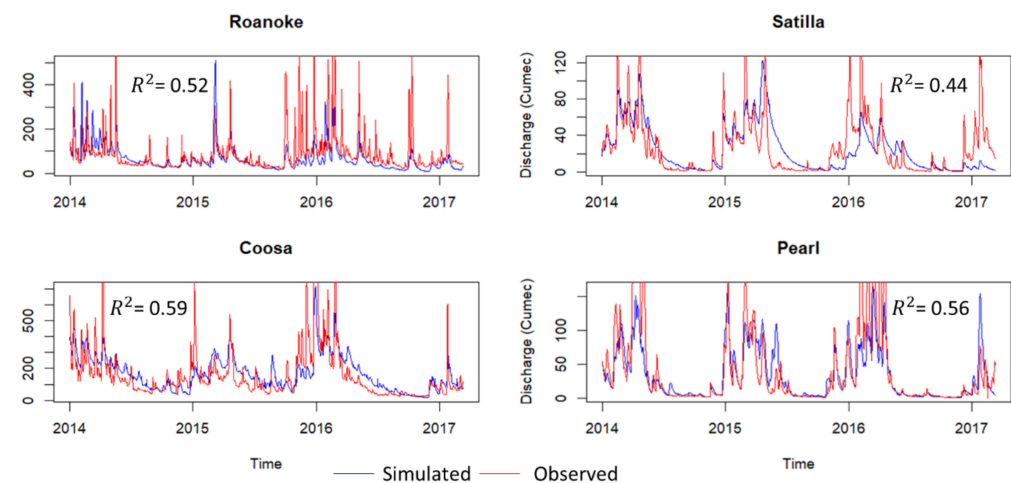


Figure 8. Observed vs. simulated daily discharge time series using the CFSv2 integrated SWAT model at the outlet for four selected watersheds from 1 January 2014 to 12 March 2017, using near real-time data.

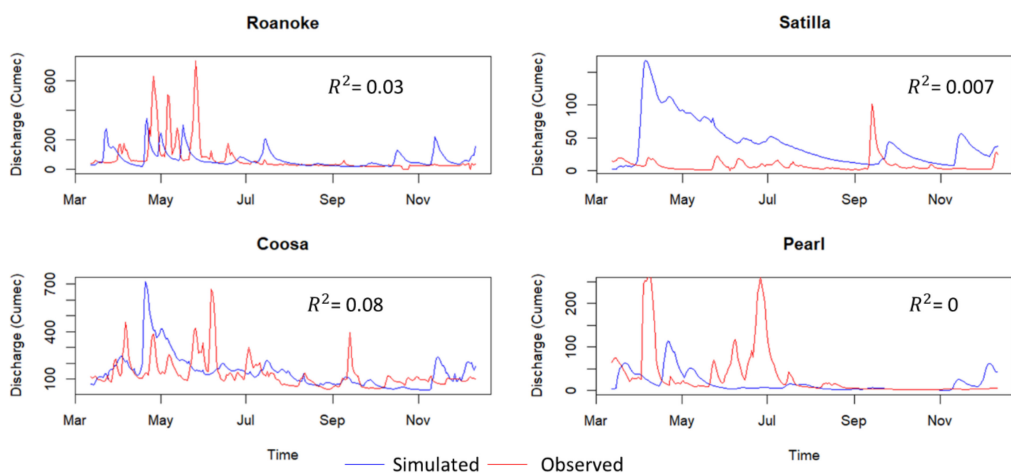


Figure 9. Observed vs. simulated daily discharge time series using the CFSv2 integrated SWAT model at the outlet for four selected watersheds using the 9-month forecast data from 13 March 2017 to 12 December 2017. Note the low values of forecasted streamflow using the SWAT-CFSv2 model for the 9-month lead time.

5.4. Water Budget Analysis for the SAG Region

Figure 10 shows the monthly water budget for the 50 watersheds in the study summarized in the form of a box plot to capture the mean, median, and variability within individual components. Most watersheds in the study region received precipitation during the summer (June–August). With high temperatures and available moisture, precipitation in the summer rose to its peak value. Soil water remained relatively consistent in the region, with a minor dip during summer months. High temperatures during April through to August led to higher PET compared to ET, thus causing

water-deficit conditions. Water-surplus conditions were attained with incoming precipitation in summer months and the subsequent fall in temperature in late spring and fall seasons. Figure 11 provides water budget plots for two select watersheds, namely the Roanoke and Pearl River watersheds. Differences in the water budget for the two watersheds is evident from Figure 11 and was primarily driven by the climatology of these watersheds. The Roanoke watershed received a total monthly precipitation of approximately 100 mm throughout the year. Increasing temperatures in the summer led to a fall in soil water storage. However, low temperatures and reduced plant transpiration in the late fall and winters helped bring soil water back to values above 150 mm. The Pearl River falls received the highest rainfall in summer months (June–August) and was often affected by the tropical cyclones. Soil water for the watershed consistently remained higher than 150 mm. High summer temperatures and moisture availability fueled high evapotranspiration in the watershed, especially during summers.

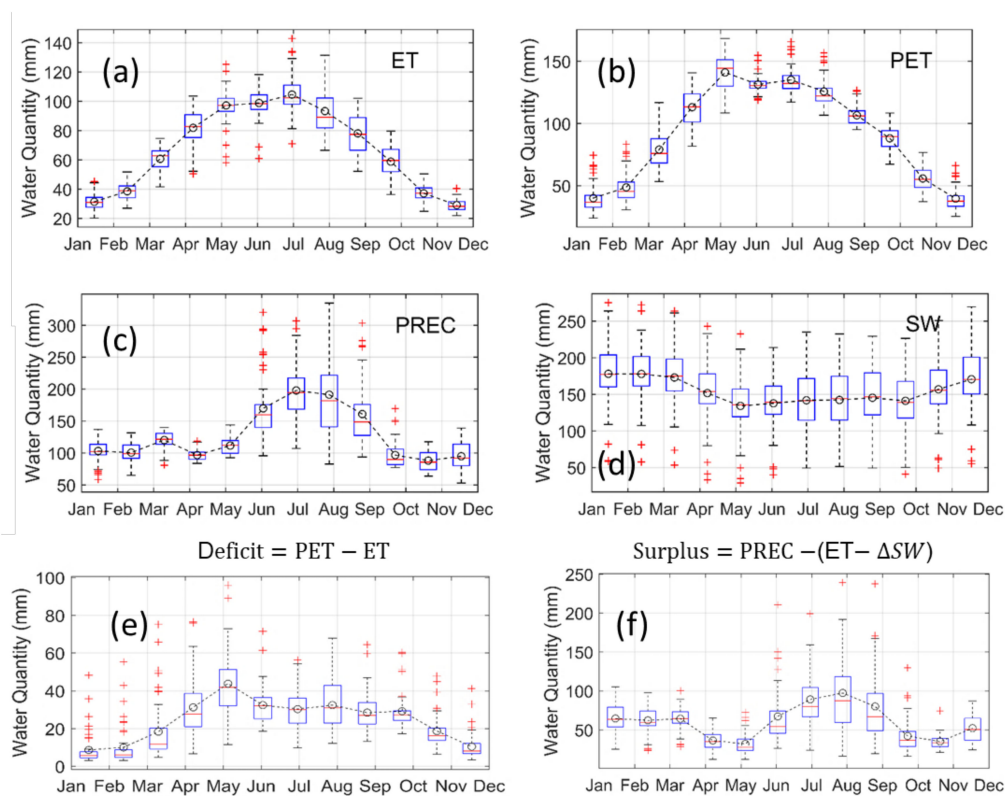


Figure 10. (a–d) Box plots of monthly water budget components for the 50 watersheds in the study area. (e,f) Box plots of monthly water deficit and surplus for the 50 watersheds. The mean for all watersheds is shown by dotted line and circles. Median is represented by a red line. (Reproduced with permission from Sehgal and Sridhar [59]).

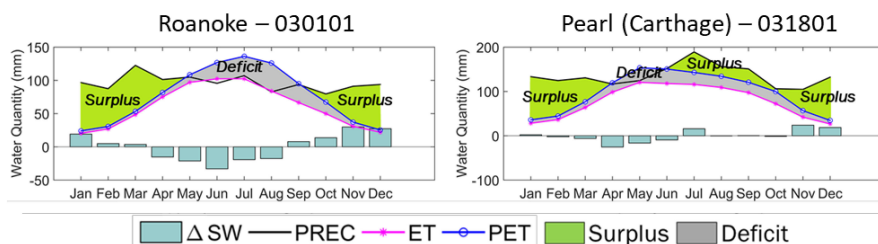


Figure 11. Monthly water budget components for the Roanoke and Pearl River watersheds. Water surplus and deficit conditions are shown with green and gray shade, respectively.

5.5. Hydrological Forecasts for South Atlantic-Gulf Region Using the CFSv2-Integrated SWAT Model

The effect of the drought in the region can be observed in Figure 12 for the year 2016, where a high PET and low soil moisture and precipitation led to water deficit conditions and hence drought in the SEUS. Dry conditions affected large parts of the study region, predominantly Alabama, Georgia, Florida, and many parts of North and South Carolina, leading to severe drought conditions in the affected regions. A similar condition was expected to be observed in July and August 2017, with relief due to forecasted precipitation in the region in the later part of the year. Spatial maps of the forecasted values of PREC, PET, ET, and soil water storage (SW) are provided in Figure 12. The spatial variability in the hydrologic variables is evident from Figure 12, which is strongly influenced by seasonality and hydroclimatology. Summer temperatures led to high PET and ET and low soil moisture in the region from May through to August. High spatial variability can be seen in the case of precipitation, where parts of Louisiana, Alabama, and Georgia were expected to receive higher precipitation during April and May, whereas many parts of Florida and the Carolinas receive precipitation during July through November. For interested readers, the observed total precipitation for the study region is provided from April–December 2017 in Figure S8.1 of the Supplementary Material.

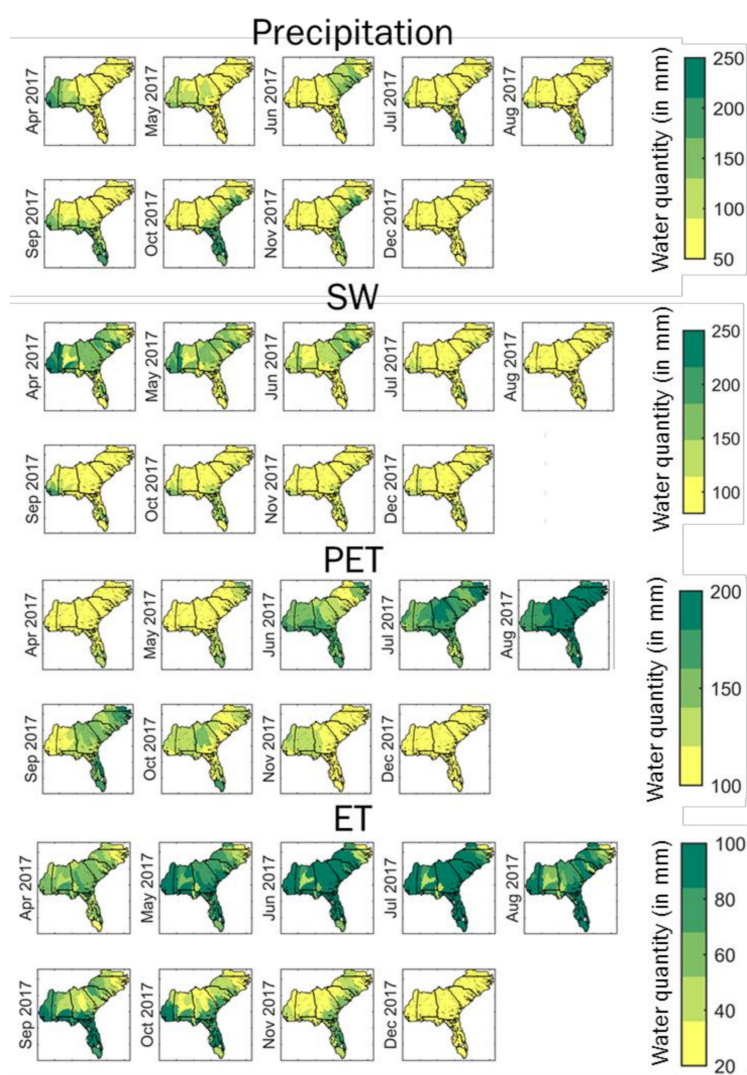


Figure 12. Spatial plots of forecasted monthly average values of precipitation (PREC), actual evapotranspiration (ET), potential evapotranspiration (PET), and soil water storage (SW) for the SAG region.

5.6. Uncertainty in Model Outputs

Data, model, and parametric uncertainty are three main causes of errors in hydrological models. Model uncertainties can be a result of measurement errors associated with the model inputs (DEM, land use classification), from the model structure and its assumptions and simplification, and from approximations in determining parameters [99,100]. Parameter uncertainty, among other sources, is highly likely because of lack of availability of the measured parameters (e.g., soil hydraulic properties and basin characteristics, etc.). Calibrating models for the best parameters may also have issues such as equifinality [101] (different parameter sets resulting in similar model results), due to interactions and interrelationships between the parameters. This is specifically true for heavily managed watersheds in some parts of the study region where the model parameters adjust for anthropogenic influence on the watershed without any explicit inclusion of management practices in the design or implementation of the hydrologic model. The issue of equifinality and parametric uncertainty in the SWAT model is well discussed in the literature [102–104].

The performance of the SWAT-CFSv2 simulations also depend heavily on the forecasting ability of the CFSv2 weather data for the region of analysis. Several other studies have highlighted the issue of uncertainty in CFSv2 models and their influence on the simulation of various hydrologic models. Zhang et al. [55] tested the efficiency of VIC models initialized with satellite-aided monitoring (MONIT), CFSv2, and ensemble streamflow prediction (ESP), and evaluated the performance of the soil moisture forecast skill and observed that the uncertainty in the soil moisture forecast is mostly controlled by initial conditions in the first month and that uncertainties in the CFSv2 climate forecasts have the largest contribution to SM forecast errors at longer lead times. Furthermore, seasonality hydroclimatological variations have a significant impact on the modeling performance of CFSv2 models [105–107]. In other words, the hydrological predictions using SWAT-CFSv2 may be more skillful in some seasons compared to others due to the combined influence of teleconnections with large-scale climatic drivers, which may lead to a more predictable influence on the water budget of the study area (hurricanes and high precipitation or increased temperatures and reduced precipitation, etc.).

6. Conclusions

This study provides an important platform for generating high-resolution hydrologic simulations for the southeastern U.S. at high spatial (HUC-12) and temporal (daily) resolution, which can be of importance to water planners and policymakers of the region. The models were calibrated using the SUFI-2 algorithm module in SWAT-CUP for the period of January 2001–December 2010 and validated through to December 2013 at a daily time step using observed streamflow datasets from USGS.

From the calibrated model, we generated the water budget components for 50 watersheds in the South Atlantic-Gulf region of the southeastern US from January 1982–December 2013 using the CFSR meteorological dataset. In addition, we provided a framework for near real-time forecasting of hydrologic variables in the study area by integrating the SWAT model with meteorological drivers from CFSv2 climate forecast models with a lead time of 9 months. The CFSv2-integrated SWAT model estimated soil moisture and other hydrologic outputs corresponding to the near real-time CFSv2 model simulation output from January 2014 through to March 2017 and forecasted values for 9 months through to December 2017.

The results have been carefully evaluated by several quantitative and subjective approaches. Observed streamflow and in-situ soil moisture datasets were used to provide a statistical estimation of the accuracy of the model simulations, whereas the influence of land use on calibrated parameters, the complementary relationship between ET and PET [108,109], and the water balance of the study region were studied in order to gain confidence in the model simulations. The results indicated that the models were effective in capturing the hydrologic variability in the implemented watershed in terms of high accuracy in simulating streamflow discharge for 50 outlet points and a satisfactory correlation with the in-situ soil moisture dataset from nine stations across the region for the total rooting depth soil profile. The near real-time simulations using the CFSv2-integrated SWAT model were found to be

satisfactory. However, the hydrological forecasts made using the forecasted meteorological dataset from CFSv2 needs improvement for longer lead time periods. The hydrological forecasts from the CFSv2-integrated SWAT model were found to be reasonable for a lead time of approximately 1 month, beyond which the uncertainty in the models render the hydrological forecast unreliable. However, regularly updating the integrated SWAT-CFSv2 models on a weekly/bi-weekly basis could help solve this shortcoming. Insights into the watershed-scale hydrological processes over the vast regions of the SEUS are useful for water planners and policymakers of the region, which is increasingly prone to water scarcity in the wake of high (and growing) agricultural and industrial water demand. As a follow-on study, the simulated dataset will be subsequently evaluated for varied applications such as drought monitoring and forecasting, flood/forest fire risk assessments, and other applications related to agricultural and water resources.

Supplementary Materials: The following are available online at <http://www.mdpi.com/2071-1050/10/9/3079/s1>, S1: Climatology (average annual precipitation, and maximum and minimum annual temperatures) of 50 watersheds based on 1979–2013 data; S2: Flow hydrographs: SWAT simulation versus USGS observed discharge; S3: Performance statistics of the SWAT model calibration and validation for 50 watersheds; S4: Watershed-scale water balance plots from simulated hydrologic variables using calibrated SWAT model implementation for the period January 1982–December 2013; S5: Time series of soil moisture from an in-situ station; S6: Modeling evapotranspiration; S7: Watershed-scale time series of the forecasted hydrologic variables (precipitation, actual evapotranspiration, potential evapotranspiration, and soil moisture) simulated using SWAT-CFSv2 hybrid models.

Author Contributions: Conceptualization, V.S. and V.R.S.; Methodology, V.R.S.; Software, V.S.; Validation, V.S., V.R.S.; Data Curation, V.S. and V.R.S.; Writing—Original Draft Preparation, V.S.; Writing—Review and Editing, V.R.S., J.A.O., L.J., V.S.; Supervision, V.R.S.; Project Administration, V.R.S.; Funding Acquisition, V.R.S.

Funding: This project was funded, in part, by the Virginia Agricultural Experiment Station (Blacksburg) and the Hatch Program of the National Institute of Food and Agriculture, U.S. Department of Agriculture (Washington, D.C.).

Conflicts of Interest: The authors declare no conflict of interest.

Abbreviations

| | |
|--------|---|
| SWAT | Soil and Water Assessment Tool |
| SM | Soil moisture |
| ET | Actual Evapotranspiration |
| PET | Potential Evapotranspiration |
| HUC-12 | A 12-digit Hydrologic Unit Code |
| USGS | U.S. Geological Survey |
| USCRN | U.S. Climate Reference Network |
| CFSv2 | National Centers for Environmental Prediction coupled forecast system model version 2 |

References

1. Mu, Q.; Zhao, M.; Kimball, J.S.; McDowell, N.G.; Running, S.W. A remotely sensed global terrestrial drought severity index. *Bull. Am. Meteorol. Soc.* **2013**, *94*, 83–98. [[CrossRef](#)]
2. Hanjra, M.A.; Qureshi, M.E. Global water crisis and future food security in an era of climate change. *Food Policy* **2010**, *35*, 365–377. [[CrossRef](#)]
3. Sheffield, J.; Wood, E.F.; Chaney, N.; Guan, K.; Sadri, S.; Yuan, X.; Olang, L.; Amani, A.; Ali, A.; Demuth, S. A drought monitoring and forecasting system for sub-Saharan African water resources and food security. *Bull. Am. Meteorol. Soc.* **2014**, *95*, 861–882. [[CrossRef](#)]
4. Pederson, N.; Bell, A.R.; Knight, T.A.; Leland, C.; Malcomb, N.; Anchukaitis, K.J.; Tackett, K.; Scheff, J.; Brice, A.; Catron, B. A long-term perspective on a modern drought in the American southeast. *Environ. Res. Lett.* **2012**, *7*, 014034. [[CrossRef](#)]
5. Manuel, J. Drought in the southeast: Lessons for water management. *Environ. Health Perspect.* **2008**, *116*, 168–171. [[CrossRef](#)]
6. Seager, R.; Tzanova, A.; Nakamura, J. Drought in the southeastern United States: Causes, variability over the last millennium, and the potential for future hydroclimate change. *J. Clim.* **2009**, *22*, 5021–5045. [[CrossRef](#)]

7. Nagy, R.; Lockaby, B.G.; Helms, B.; Kalin, L.; Stoeckel, D. Water resources and land use and cover in a humid region: The southeastern United States. *J. Environ. Qual.* **2011**, *40*, 867–878. [[CrossRef](#)] [[PubMed](#)]
8. U.S. Census Bureau. *Interim State Population Projections*; U.S. Census Bureau: Washington, DC, USA, 2005.
9. Scasta, J.D.; Weir, J.R.; Stambaugh, M.C. Droughts and wildfires in western us rangelands. *Rangelands* **2016**, *38*, 197–203. [[CrossRef](#)]
10. Madadgar, S.; Moradkhani, H. Spatio-temporal drought forecasting within Bayesian networks. *J. Hydrol.* **2014**, *512*, 134–146. [[CrossRef](#)]
11. Lu, J.; Sun, G.; McNulty, S.G.; Amatya, D.M. Modeling actual evapotranspiration from forested watersheds across the southeastern united states. *J. Am. Water Resour. Assoc.* **2003**, *39*, 886–896. [[CrossRef](#)]
12. Limaye, A.S.; Boyington, T.M.; Cruise, J.F.; Bulusu, A.; Brown, E. Macroscale hydrologic modeling for regional climate assessment studies in the southeastern united states. *J. Am. Water Resour. Assoc.* **2001**, *37*, 709–722. [[CrossRef](#)]
13. Sun, S.; Chen, B.; Shao, Q.; Chen, J.; Liu, J.; Zhang, X.-j.Z.; Zhang, H.; Lin, X. Modeling evapotranspiration over China’s landmass from 1979 to 2012 using multiple land surface models: Evaluations and analyses. *J. Hydrometeorol.* **2017**, *18*, 1185–1203. [[CrossRef](#)]
14. Ciabatta, L.; Brocca, L.; Massari, C.; Moramarco, T.; Gabellani, S.; Puca, S.; Wagner, W. Rainfall-runoff modelling by using sm2rain-derived and state-of-the-art satellite rainfall products over Italy. *Int. J. Appl. Earth Obs. Geoinf.* **2016**, *48*, 163–173. [[CrossRef](#)]
15. Brocca, L.; Melone, F.; Moramarco, T.; Wagner, W.; Naeimi, V.; Bartalis, Z.; Hasenauer, S. Improving runoff prediction through the assimilation of the ascat soil moisture product. *Hydrol. Earth Syst. Sci.* **2010**, *14*, 1881–1893. [[CrossRef](#)]
16. Laiolo, P.; Gabellani, S.; Campo, L.; Silvestro, F.; Delogu, F.; Rudari, R.; Pulvirenti, L.; Boni, G.; Fascetti, F.; Pierdicca, N. Impact of different satellite soil moisture products on the predictions of a continuous distributed hydrological model. *Int. J. Appl. Earth Obs. Geoinf.* **2016**, *48*, 131–145. [[CrossRef](#)]
17. Bangira, T.; Maathuis, B.H.; Dube, T.; Gara, T.W. Investigating flash floods potential areas using ascat and trmm satellites in the western cape province, South Africa. *Geocartol. Int.* **2015**, *30*, 737–754. [[CrossRef](#)]
18. Alvarez-Garreton, C.; Ryu, D.; Western, A.; Su, C.-H.; Crow, W.; Robertson, D.; Leahy, C. Improving operational flood ensemble prediction by the assimilation of satellite soil moisture: Comparison between lumped and semi-distributed schemes. *Hydrol. Earth Syst. Sci.* **2015**, *19*, 1659–1676. [[CrossRef](#)]
19. Nanda, T.; Sahoo, B.; Beria, H.; Chatterjee, C. A wavelet-based non-linear autoregressive with exogenous inputs (wnarx) dynamic neural network model for real-time flood forecasting using satellite—Based rainfall products. *J. Hydrol.* **2016**, *539*, 57–73. [[CrossRef](#)]
20. Hobbins, M.T.; Wood, A.; McEvoy, D.J.; Huntington, J.L.; Morton, C.; Anderson, M.; Hain, C. The evaporative demand drought index. Part i: Linking drought evolution to variations in evaporative demand. *J. Hydrometeorol.* **2016**, *17*, 1745–1761. [[CrossRef](#)]
21. Anderson, M.C.; Norman, J.M.; Mecikalski, J.R.; Otkin, J.A.; Kustas, W.P. A climatological study of evapotranspiration and moisture stress across the continental United States based on thermal remote sensing: 1. Model formulation. *J. Geophys. Res. Atmos.* **2007**, *112*. [[CrossRef](#)]
22. Sridhar, V.; Hubbard, K.G.; You, J.; Hunt, E.D. Development of the soil moisture index to quantify agricultural drought and its “user friendliness” in severity-area-duration assessment. *J. Hydrometeorol.* **2008**, *9*, 660–676. [[CrossRef](#)]
23. Zhang, Y.; Peña-Arancibia, J.L.; McVicar, T.R.; Chiew, F.H.; Vaze, J.; Liu, C.; Lu, X.; Zheng, H.; Wang, Y.; Liu, Y.Y. Multi-decadal trends in global terrestrial evapotranspiration and its components. *Sci. Rep.* **2016**, *6*, 19124. [[CrossRef](#)] [[PubMed](#)]
24. Mao, J.; Fu, W.; Shi, X.; Ricciuto, D.M.; Fisher, J.B.; Dickinson, R.E.; Wei, Y.; Shem, W.; Piao, S.; Wang, K. Disentangling climatic and anthropogenic controls on global terrestrial evapotranspiration trends. *Environ. Res. Lett.* **2015**, *10*, 094008. [[CrossRef](#)]
25. Sehgal, V. Near Real-Time Seasonal Drought Forecasting and Retrospective Drought Analysis Using Simulated Multi-Layer Soil Moisture From Hydrological Models at Sub-Watershed Scales. Master’s Thesis, Virginia Tech, Blacksburg, VA, USA, 2017.
26. Sehgal, V.; Sridhar, V.; Tyagi, A. Stratified drought analysis using a stochastic ensemble of simulated and in-situ soil moisture observations. *J. Hydrol.* **2017**, *545*, 226–250. [[CrossRef](#)]

27. Sridhar, V.; Elliott, R.L.; Chen, F. Scaling effects on modeled surface energy-balance components using the noah-osu land surface model. *J. Hydrol.* **2003**, *280*, 105–123. [[CrossRef](#)]
28. Sridhar, V.; Anderson, K. Human-induced modifications to boundary layer fluxes and their water management implications in a changing climate. *Agric. For. Meteorol.* **2017**, *234*, 66–79. [[CrossRef](#)]
29. Garnaud, C.; Bélair, S.; Carrera, M.L.; McNairn, H.; Pacheco, A. Field-scale spatial variability of soil moisture and l-band brightness temperature from land surface modeling. *J. Hydrometeorol.* **2017**, *18*, 573–589. [[CrossRef](#)]
30. Jimenez, C.; Prigent, C.; Aires, F. Toward an estimation of global land surface heat fluxes from multisatellite observations. *J. Geophys. Res. Atmos.* **2009**, *114*. [[CrossRef](#)]
31. Jung, M.; Reichstein, M.; Bondeau, A. Towards global empirical upscaling of fluxnet eddy covariance observations: Validation of a model tree ensemble approach using a biosphere model. *Biogeosciences* **2009**, *6*, 2001–2013.
32. Zhang, Y.; Leuning, R.; Hutley, L.B.; Beringer, J.; McHugh, I.; Walker, J.P. Using long-term water balances to parameterize surface conductances and calculate evaporation at 0.05 spatial resolution. *Water Resour. Res.* **2010**, *46*. [[CrossRef](#)]
33. Mueller, B.; Seneviratne, S.; Jimenez, C.; Corti, T.; Hirschi, M.; Balsamo, G.; Ciais, P.; Dirmeyer, P.; Fisher, J.; Guo, Z. Evaluation of global observations-based evapotranspiration datasets and ipcc ar4 simulations. *Geophys. Res. Lett.* **2011**, *38*. [[CrossRef](#)]
34. Vinukollu, R.K.; Wood, E.F.; Ferguson, C.R.; Fisher, J.B. Global estimates of evapotranspiration for climate studies using multi-sensor remote sensing data: Evaluation of three process-based approaches. *Remote Sens. Environ.* **2011**, *115*, 801–823. [[CrossRef](#)]
35. Polhamus, A.; Fisher, J.B.; Tu, K.P. What controls the error structure in evapotranspiration models? *Agric. For. Meteorol.* **2013**, *169*, 12–24. [[CrossRef](#)]
36. Muttiah, R.S.; Wurbs, R.A. Scale-dependent soil and climate variability effects on watershed water balance of the swat model. *J. Hydrol.* **2002**, *256*, 264–285. [[CrossRef](#)]
37. Cao, W.; Bowden, W.B.; Davie, T.; Fenemor, A. Multi-variable and multi-site calibration and validation of swat in a large mountainous catchment with high spatial variability. *Hydrol. Process.* **2006**, *20*, 1057–1073. [[CrossRef](#)]
38. Xu, Z.; Pang, J.; Liu, C.; Li, J. Assessment of runoff and sediment yield in the miyun reservoir catchment by using swat model. *Hydrol. Process.* **2009**, *23*, 3619–3630. [[CrossRef](#)]
39. Yan, D.; Shi, X.; Yang, Z.; Li, Y.; Zhao, K.; Yuan, Y. Modified palmer drought severity index based on distributed hydrological simulation. *Math. Probl. Eng.* **2013**, *2013*, 327374. [[CrossRef](#)]
40. Marek, G.W.; Gowda, P.H.; Evett, S.R.; Baumhardt, R.L.; Brauer, D.K.; Howell, T.A.; Marek, T.H.; Srinivasan, R. Estimating evapotranspiration for dryland cropping systems in the semiarid Texas high plains using swat. *JAWRA J. Am. Water Resour. Assoc.* **2016**, *52*, 298–314. [[CrossRef](#)]
41. Wetterhall, F.; Winsemius, H.; Dutra, E.; Werner, M.; Pappenberger, E. Seasonal predictions of agro-meteorological drought indicators for the Limpopo basin. *Hydrol. Earth Syst. Sci.* **2015**, *19*, 2577–2586. [[CrossRef](#)]
42. Shah, R.D.; Mishra, V. Utility of global ensemble forecast system (gefs) reforecast for medium-range drought prediction in India. *J. Hydrometeorol.* **2016**, *17*, 1781–1800. [[CrossRef](#)]
43. Hansen, J.W. Integrating seasonal climate prediction and agricultural models for insights into agricultural practice. *Philos. Trans. R. Soc. Lond. B Biol. Sci.* **2005**, *360*, 2037–2047. [[CrossRef](#)] [[PubMed](#)]
44. Shafiee-Jood, M.; Cai, X.; Chen, L.; Liang, X.Z.; Kumar, P. Assessing the value of seasonal climate forecast information through an end-to-end forecasting framework: Application to us 2012 drought in central Illinois. *Water Resour. Res.* **2014**, *50*, 6592–6609. [[CrossRef](#)]
45. Dutra, E.; Magnusson, L.; Wetterhall, F.; Cloke, H.L.; Balsamo, G.; Bousssetta, S.; Pappenberger, F. The 2010–2011 drought in the horn of Africa in ecmwf reanalysis and seasonal forecast products. *Int. J. Climatol.* **2013**, *33*, 1720–1729. [[CrossRef](#)]
46. Ma, F.; Yuan, X.; Ye, A. Seasonal drought predictability and forecast skill over china. *J. Geophys. Res. Atmos.* **2015**, *120*, 8264–8275. [[CrossRef](#)]
47. Crane, T.A.; Roncoli, C.; Paz, J.; Breuer, N.; Broad, K.; Ingram, K.T.; Hoogenboom, G. Forecast skill and farmers' skills: Seasonal climate forecasts and agricultural risk management in the southeastern United States. *Weather Clim. Soc.* **2010**, *2*, 44–59. [[CrossRef](#)]

48. Gunda, T.; Bazuin, J.; Nay, J.; Yeung, K. Impact of seasonal forecast use on agricultural income in a system with varying crop costs and returns: An empirically-grounded simulation. *Environ. Res. Lett.* **2017**, *12*, 034001. [[CrossRef](#)]
49. Mo, K.C.; Long, L.N.; Xia, Y.; Yang, S.; Schemm, J.E.; Ek, M. Drought indices based on the climate forecast system reanalysis and ensemble nldas. *J. Hydrometeorol.* **2011**, *12*, 181–205. [[CrossRef](#)]
50. Dirmeyer, P.A. Characteristics of the water cycle and land–atmosphere interactions from a comprehensive reforecast and reanalysis data set: Cfsv2. *Clim. Dyn.* **2013**, *41*, 1083–1097. [[CrossRef](#)]
51. McEvoy, D.J.; Huntington, J.L.; Mejia, J.F.; Hobbins, M.T. Improved seasonal drought forecasts using reference evapotranspiration anomalies. *Geophys. Res. Lett.* **2016**, *43*, 377–385. [[CrossRef](#)]
52. Mo, K.C.; Shukla, S.; Lettenmaier, D.P.; Chen, L.C. Do climate forecast system (cfsv2) forecasts improve seasonal soil moisture prediction? *Geophys. Res. Lett.* **2012**, *39*. [[CrossRef](#)]
53. Roundy, J.K.; Ferguson, C.R.; Wood, E.F. Impact of land-atmospheric coupling in cfsv2 on drought prediction. *Clim. Dyn.* **2014**, *43*, 421–434. [[CrossRef](#)]
54. Mace, R.E.; Yang, B.; Pu, B. *Early Warning of Summer Drought over Texas and the South Central United States: Spring Conditions as a Harbinger of Summer Drought*; Technical note; Texas Water Development Board, Austin: Austin, TX, USA, 2015.
55. Zhang, X.; Tang, Q.; Liu, X.; Leng, G.; Li, Z. Soil moisture drought monitoring and forecasting using satellite and climate model data over southwestern China. *J. Hydrometeorol.* **2017**, *18*, 5–23. [[CrossRef](#)]
56. Saha, S.; Moorthi, S.; Pan, H.-L.; Wu, X.; Wang, J.; Nadiga, S.; Tripp, P.; Kistler, R.; Woollen, J.; Behringer, D. The ncep climate forecast system reanalysis. *Bull. Am. Meteorol. Soc.* **2010**, *91*, 1015–1058. [[CrossRef](#)]
57. Kang, H.; Sridhar, V. Improved drought prediction using near real-time climate forecasts and simulated hydrologic conditions. *Sustainability* **2018**, *10*, 1799. [[CrossRef](#)]
58. Kang, H.; Sridhar, V. Combined statistical and spatially distributed hydrological model for evaluating future drought indices in Virginia. *J. Hydrol. Reg. Stud.* **2017**, *12*, 253–272. [[CrossRef](#)]
59. Sehgal, V.; Sridhar, V. Effect of hydroclimatological teleconnections on the watershed-scale drought predictability in the southeastern US. *Int. J. Climatol.* **2018**, *38*, e1139–e1157. [[CrossRef](#)]
60. Suliman, A.H.A.; Jajarmizadeh, M.; Harun, S.; Darus, I.Z.M. Comparison of semi-distributed, gis-based hydrological models for the prediction of streamflow in a large catchment. *Water Resour. Manag.* **2015**, *29*, 3095–3110. [[CrossRef](#)]
61. Neitsch, S.L.; Arnold, J.G.; Kiniry, J.R.; Williams, J.R. *Soil and Water Assessment Tool Theoretical Documentation Version 2009*; Texas Water Resources Institute, Texas A&M University: College Station, TX, USA, 2011.
62. Arnold, J.G.; Moriasi, D.N.; Gassman, P.W.; Abbaspour, K.C.; White, M.J.; Srinivasan, R.; Santhi, C.; Harmel, R.; Van Griensven, A.; Van Liew, M.W. Swat: Model use, calibration, and validation. *Trans. ASABE* **2012**, *55*, 1491–1508. [[CrossRef](#)]
63. Gassman, P.; Reyes, M.; Green, C.; Arnold, J. The soil and water assessment tool: Historical development, applications, and future research directions. *Trans. Am. Soc. Agric. Biol. Eng.* **2007**, *50*, 1211–1250. [[CrossRef](#)]
64. Arnold, J.G.; Srinivasan, R.; Muttiah, R.S.; Williams, J.R. Large area hydrologic modeling and assessment part i: model development1. *J. Am. Water Resour. Assoc.* **1998**, *34*, 73–89. [[CrossRef](#)]
65. Liu, Y.; Yang, W.; Wang, X. Development of a swat extension module to simulate riparian wetland hydrologic processes at a watershed scale. *Hydrol. Process.* **2008**, *22*, 2901–2915. [[CrossRef](#)]
66. Williams, J.; Jones, C.; Dyke, P. A modeling approach to determining the relationship between erosion and soil productivity. *Trans. ASAE* **1984**, *27*, 129–144. [[CrossRef](#)]
67. SWAT. *Swat Literature Database for Peer-Reviewed Journal Articles*; Center for Agricultural and Rural Development: Ames, IA, USA, 2017.
68. United States Geological Survey. *Boundary Descriptions and Names of Regions, Subregions, Accounting Units and Cataloging Units*; USGS: Reston, NA, USA, 2017.
69. McEvoy, D.J. Physically Based Evaporative Demand as a Drought Metric: Historical Analysis and Seasonal Prediction. Ph.D. Thesis, University of Nevada, Reno, NV, USA, 2015.

70. Homer, C.G.; Dewitz, J.A.; Yang, L.; Jin, S.; Danielson, P.; Xian, G.; Coulston, J.; Herold, N.D.; Wickham, J.; Megown, K. Completion of the 2011 national land cover database for the conterminous united states-representing a decade of land cover change information. *Photogramm. Eng. Remote Sens.* **2015**, *81*, 345–354.
71. Dile, Y.T.; Srinivasan, R. Evaluation of cfsr climate data for hydrologic prediction in data-scarce watersheds: An application in the blue Nile river basin. *JAWRA J. Am. Water Resour. Assoc.* **2014**, *50*, 1226–1241. [[CrossRef](#)]
72. Tuo, Y.; Duan, Z.; Disse, M.; Chiogna, G. Evaluation of precipitation input for SWAT modeling in Alpine catchment: A case study in the Adige river basin (Italy). *Sci. Total Environ.* **2016**, *573*, 66–82. [[CrossRef](#)] [[PubMed](#)]
73. Vu, M.; Raghavan, S.V.; Liong, S.Y. Swat use of gridded observations for simulating runoff—a Vietnam river basin study. *Hydrol. Earth Syst. Sci.* **2012**, *16*, 2801–2811. [[CrossRef](#)]
74. Duethmann, D.; Zimmer, J.; Gafurov, A.; Güntner, A.; Kriegel, D.; Merz, B.; Vorogushyn, S. Evaluation of areal precipitation estimates based on downscaled reanalysis and station data by hydrological modelling. *Hydrol. Earth Syst. Sci.* **2013**, *17*, 2415–2434. [[CrossRef](#)]
75. Yang, Y.; Wang, G.; Wang, L.; Yu, J.; Xu, Z. Evaluation of gridded precipitation data for driving swat model in area upstream of three gorges reservoir. *PLoS ONE* **2014**, *9*, e112725. [[CrossRef](#)] [[PubMed](#)]
76. Abbaspour, K.C.; van Genuchten, M.T.; Schulin, R.; Schläppi, E. A sequential uncertainty domain inverse procedure for estimating subsurface flow and transport parameters. *Water Resour. Res.* **1997**, *33*, 1879–1892. [[CrossRef](#)]
77. Abbaspour, K.; Johnson, C.; Van Genuchten, M.T. Estimating uncertain flow and transport parameters using a sequential uncertainty fitting procedure. *Vadose Zone J.* **2004**, *3*, 1340–1352. [[CrossRef](#)]
78. Abbaspour, K.; Rouholahnejad, E.; Vaghefi, S.; Srinivasan, R.; Yang, H.; Kløve, B. A continental-scale hydrology and water quality model for Europe: Calibration and uncertainty of a high-resolution large-scale swat model. *J. Hydrol.* **2015**, *524*, 733–752. [[CrossRef](#)]
79. Jin, X.; Sridhar, V. Impacts of climate change on hydrology and water resources in the Boise and Spokane river basins1. *JAWRA J. Am. Water Resour. Assoc.* **2012**, *48*, 197–220. [[CrossRef](#)]
80. Rouholahnejad, E.; Abbaspour, K.C.; Vejdani, M.; Srinivasan, R.; Schulin, R.; Lehmann, A. A parallelization framework for calibration of hydrological models. *Environ. Model. Softw.* **2012**, *31*, 28–36. [[CrossRef](#)]
81. Nash, J.E.; Sutcliffe, J.V. River flow forecasting through conceptual models part i—A discussion of principles. *J. Hydrol.* **1970**, *10*, 282–290. [[CrossRef](#)]
82. Feyereisen, G.; Strickland, T.; Bosch, D.; Sullivan, D. Evaluation of swat manual calibration and input parameter sensitivity in the little river watershed. *Trans. ASABE* **2007**, *50*, 843–855. [[CrossRef](#)]
83. Kang, H.; Sridhar, V. A statistical and distributed hydrological modeling combination to evaluate drought indices in Virginia. *JAWRA J. Am. Water Resour. Assoc.* **2017**. [[CrossRef](#)]
84. Wang, X.; Yang, W.; Melesse, A.M. Using hydrologic equivalent wetland concept within swat to estimate streamflow in watersheds with numerous Wetlands. *Trans. ASAE* **2008**, *51*, 55–72. [[CrossRef](#)]
85. Van Liew, M.W.; Arnold, J.; Bosch, D. Problems and potential of autocalibrating a hydrologic model. *Trans. ASAE* **2005**, *48*, 1025–1040. [[CrossRef](#)]
86. Uniyal, B.; Jha, M.K.; Verma, A.K. Parameter identification and uncertainty analysis for simulating streamflow in a river basin of eastern India. *Hydrol. Process.* **2015**, *29*, 3744–3766. [[CrossRef](#)]
87. Kang, H.; Moon, J.; Shin, Y.; Ryu, J.; Kum, D.H.; Jang, C.; Choi, J.; Kong, D.S.; Lim, K.J. Modification of swat auto-calibration for accurate flow estimation at all flow regimes. *Paddy Water Environ.* **2016**, *14*, 499–508. [[CrossRef](#)]
88. Martinez-Martinez, E.; Nejadhashemi, A.P.; Woznicki, S.A.; Love, B.J. Modeling the hydrological significance of wetland restoration scenarios. *J. Environ. Manag.* **2014**, *133*, 121–134. [[CrossRef](#)] [[PubMed](#)]
89. Hovenga, P.A.; Wang, D.; Medeiros, S.C.; Hagen, S.C.; Alizad, K. The response of runoff and sediment loading in the Apalachicola river, Florida to climate and land use land cover change. *Earth's Future* **2016**, *4*, 124–142. [[CrossRef](#)]
90. Willmott, C.J.; Robeson, S.M.; Matsuura, K. A refined index of model performance. *Int. J. Climatol.* **2012**, *32*, 2088–2094. [[CrossRef](#)]
91. Willmott, C.J.; Robeson, S.M.; Matsuura, K.; Ficklin, D.L. Assessment of three dimensionless measures of model performance. *Environ. Model. Softw.* **2015**, *73*, 167–174. [[CrossRef](#)]

92. Koch, J.; Demirel, M.C.; Stisen, S. The spatial efficiency metric (spaef): Multiple-component evaluation of spatial patterns for optimization of hydrological models. *Geosci. Model Dev.* **2018**, *11*, 1873–1886. [[CrossRef](#)]
93. Demirel, M.C.; Mai, J.; Mendiguren, G.; Koch, J.; Samaniego, L.; Stisen, S. Combining satellite data and appropriate objective functions for improved spatial pattern performance of a distributed hydrologic model. *Hydrol. Earth Syst. Sci.* **2018**, *22*, 1299–1315. [[CrossRef](#)]
94. Tauro, F.; Selker, J.; van de Giesen, N.; Abrate, T.; Uijlenhoet, R.; Porfiri, M.; Manfreda, S.; Caylor, K.; Moramarco, T.; Benveniste, J. Measurements and observations in the xxi century (moxxi): Innovation and multi-disciplinarity to sense the hydrological cycle. *Hydrol. Sci. J.* **2018**, *63*, 169–196. [[CrossRef](#)]
95. Sridhar, V.; Hubbard, K. Estimation of the water balance using observed soil water in the Nebraska sandhills. *J. Hydrol. Eng.* **2009**, *15*, 70–78. [[CrossRef](#)]
96. Singh, R.; Prasad, V.H.; Bhatt, C. Remote sensing and gis approach for assessment of the water balance of a watershed/evaluation par télédétection et sig du bilan hydrologique d'un bassin versant. *Hydrol. Sci. J.* **2004**, *49*, 131–141. [[CrossRef](#)]
97. Cho, J.; Bosch, D.; Vellidis, G.; Lowrance, R.; Strickland, T. Multi-site evaluation of hydrology component of swat in the coastal plain of southwest Georgia. *Hydrol. Process.* **2013**, *27*, 1691–1700. [[CrossRef](#)]
98. Amatya, D.; Jha, M.K. Evaluating the swat model for a low-gradient forested watershed in coastal South Carolina. *Trans. ASABE* **2011**, *54*, 2151–2163. [[CrossRef](#)]
99. Yang, J.; Reichert, P.; Abbaspour, K.; Xia, J.; Yang, H. Comparing uncertainty analysis techniques for a swat application to the chaohe basin in china. *J. Hydrol.* **2008**, *358*, 1–23. [[CrossRef](#)]
100. Wu, H. Integrated Sensitivity Analysis, Calibration, and Uncertainty Propagation Analysis Approaches for Supporting Hydrological Modeling. Ph.D. Thesis, Memorial University of Newfoundland, St. John's, NL, Canada, 2016.
101. Beven, K.; Freer, J. Equifinality, data assimilation, and uncertainty estimation in mechanistic modelling of complex environmental systems using the glue methodology. *J. Hydrol.* **2001**, *249*, 11–29. [[CrossRef](#)]
102. Moreda, F.; Koren, V.; Zhang, Z.; Reed, S.; Smith, M. Parameterization of distributed hydrological models: Learning from the experiences of lumped modeling. *J. Hydrol.* **2006**, *320*, 218–237. [[CrossRef](#)]
103. Fu, C.; James, A.L.; Yao, H. Investigations of uncertainty in swat hydrologic simulations: A case study of a Canadian Shield catchment. *Hydrol. Process.* **2015**, *29*, 4000–4017. [[CrossRef](#)]
104. Abbaspour, K.C. *Swat-Cup4: Swat Calibration and Uncertainty Programs—A User Manual*; Swiss Federal Institute of Aquatic Science and Technology, Eawag: Zurich, Switzerland, 2011.
105. Lang, Y.; Ye, A.; Gong, W.; Miao, C.; Di, Z.; Xu, J.; Liu, Y.; Luo, L.; Duan, Q. Evaluating skill of seasonal precipitation and temperature predictions of ncep cfsv2 forecasts over 17 hydroclimatic regions in china. *J. Hydrometeorol.* **2014**, *15*, 1546–1559. [[CrossRef](#)]
106. Yuan, X.; Wood, E.F.; Luo, L.; Pan, M. A first look at climate forecast system version 2 (cfsv2) for hydrological seasonal prediction. *Geophys. Res. Lett.* **2011**, *38*. [[CrossRef](#)]
107. Kim, H.-M.; Webster, P.J.; Curry, J.A. Seasonal prediction skill of ecmwf system 4 and ncep cfsv2 retrospective forecast for the northern hemisphere winter. *Clim. Dyn.* **2012**, *39*, 2957–2973. [[CrossRef](#)]
108. Sridhar, V.; Jaksa, W.T.; Huntington, J.L. Spatial mapping of evapotranspiration using the complementary relationship in the natural ecosystems. In *Evapotranspiration*; Er-Raki, S., Ed.; Nova Science Publishers, Inc.: New York, NY, USA, 2013.
109. Jaksa, W.T.; Sridhar, V.; Huntington, J.L.; Khanal, M. Evaluation of the complementary relationship using noah land surface model and north American regional reanalysis (narr) data to estimate evapotranspiration in semiarid ecosystems. *J. Hydrometeorol.* **2013**, *14*, 345–359. [[CrossRef](#)]

